



OPEN ACCESS

EDITED BY

Chris Bradley,
University of Birmingham,
United Kingdom

REVIEWED BY

Alberto Saez,
University of Barcelona, Spain
Santosh Kumar Rai,
Wadia Institute of Himalayan Geology,
India

*CORRESPONDENCE

John Houston,
✉ houston.jft@gmail.com

RECEIVED 09 October 2023

ACCEPTED 21 November 2023

PUBLISHED 18 December 2023

CITATION

Houston J (2023), The provenance and persistence of the perennial Río Loa in the Atacama Desert: links between crustal processes and surface hydrology. *Front. Earth Sci.* 11:1310088. doi: 10.3389/feart.2023.1310088

COPYRIGHT

© 2023 Houston. This is an open-access article distributed under the terms of the [Creative Commons Attribution License \(CC BY\)](https://creativecommons.org/licenses/by/4.0/). The use, distribution or reproduction in other forums is permitted, provided the original author(s) and the copyright owner(s) are credited and that the original publication in this journal is cited, in accordance with accepted academic practice. No use, distribution or reproduction is permitted which does not comply with these terms.

The provenance and persistence of the perennial Río Loa in the Atacama Desert: links between crustal processes and surface hydrology

John Houston *

Rocklea, Dorchester, United Kingdom

The Río Loa is a perennial river that crosses the Atacama Desert. A basin-wide survey enables for the first time, the hydrologic regime origin, persistence and processes to be identified. Perennial baseflow in the Ríos Loa and Salado largely originates from intra-arc aquifers which are poorly known. However, the data indicate that despite flood flow being largely confined to the summer (DJF) season, sufficient storage exists in these aquifers to maintain year-round stream flow from high-altitude, across the Atacama Desert to the coast. The intra-arc aquifers of the Western Cordillera receive recharge from time-variable precipitation infiltration and time-invariant lithospheric inputs. Lithospheric inputs potentially include slab/mantle dehydration, upper crustal melt devolatilization and/or thermally induced upflow of deeply penetrating meteoric water through buried evaporites or carbonates. Downstream, aquifers in the Pre-Andean basins variably interact with surface water, depending on location, river stage and time of year, but they do not supply significant additional sources of baseflow. Hydrochemical processes include those related to volcanic activity, soil carbonate generation, silicate weathering, CO₂ degassing and calcite precipitation. Solutes undergo concentration by evaporation, gypsum dissolution, and are further affected by localized NO₃ and SO₄ inputs and mixing with saline waters. Stable isotopes reveal subcatchment specific precipitation and evaporation, whilst carbon and tritium isotopes are used to analyze recharge sources and processes in the intra-arc aquifers and downstream mixing.

KEYWORDS

Atacama, volcanic arc, baseflow, isotope hydrology, groundwater recharge

1 Introduction

The perennial flow of the Ríos Loa and Salado crossing the Atacama Desert, considered the driest place on earth, is anomalous (Figure 1). There are no other rivers that cross the Atacama and reach the ocean between 19 and 27°S, a distance of over 700 km.

The Río Loa system is a rich ecological resource within the desert and has acted as a corridor for Paleo-Indian cultures since at least 13,000 years BP (Aldenderfer, 1989; Núñez and Grosjean, 2003; Moreno et al., 2009; Latorre et al., 2013; Pestle et al., 2015; de Porras et al., 2021). Since the beginning of the 20th century water demand has increased as much as ten-fold as a consequence of mining, agricultural and municipal demands on the river and

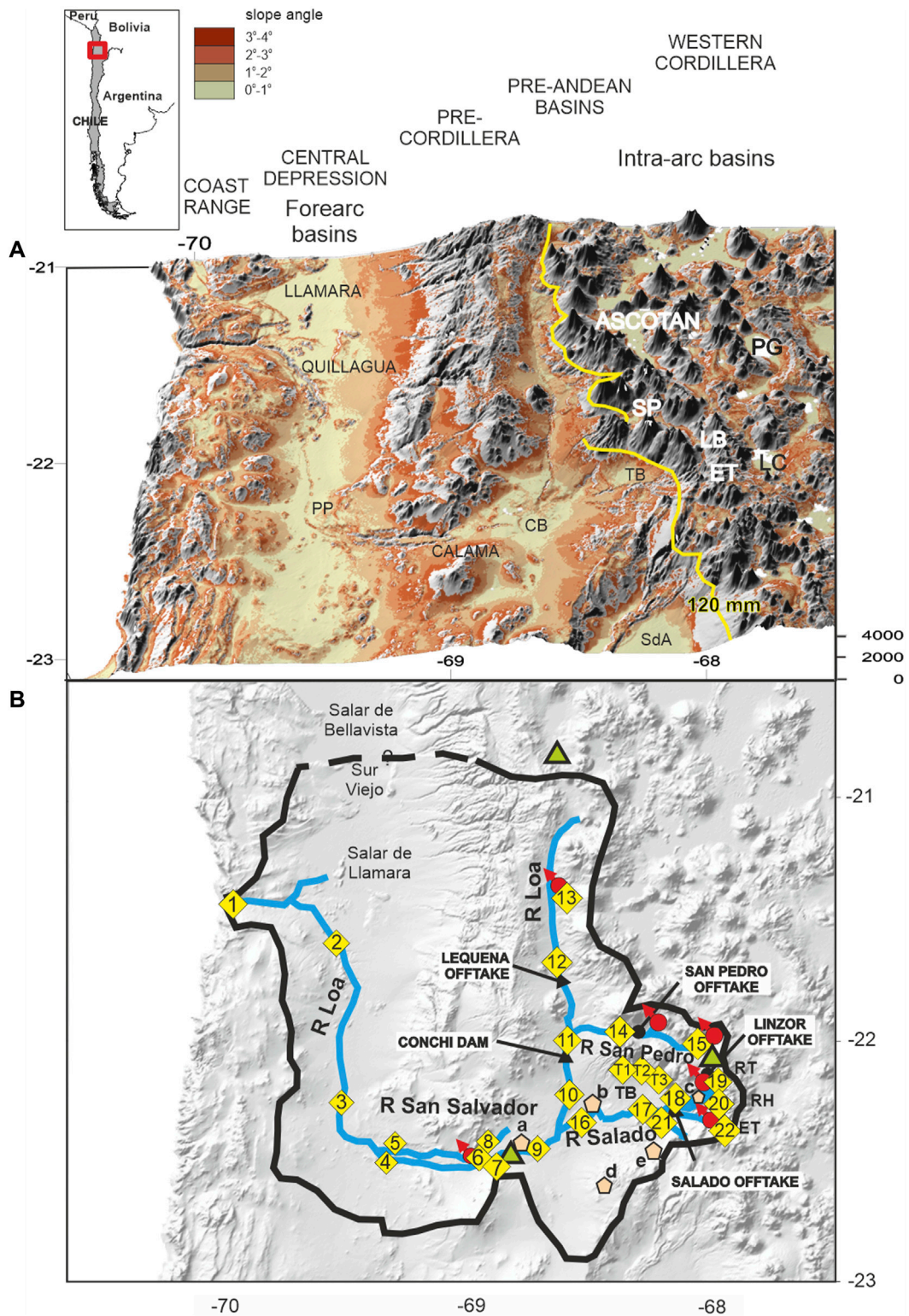


FIGURE 1

The Rio Loa catchment. **(A)** extent, location and physical features. The DEM shows the principal sedimentary basins as near flat surfaces. The yellow contour is the 120 mm/a isohyet. PP Puento Posada, CB Calama Basin, TB Turi Basin, SP San Pedro Basin, LB Linzor Basin, ET El Tatio, PG Pastos Grandes Caldera, LC Laguna Colorada. **(B)** Rio Loa catchment, surface water divide, principal abstractions and flow gauging/sample locations. Red dots represent major springs, pink polygons minor springs (a- Angostura, b- Laguna Inca Coya, c- Rio Salado, d- La Teca, e- Chitor) and green triangles rain gauge stations.

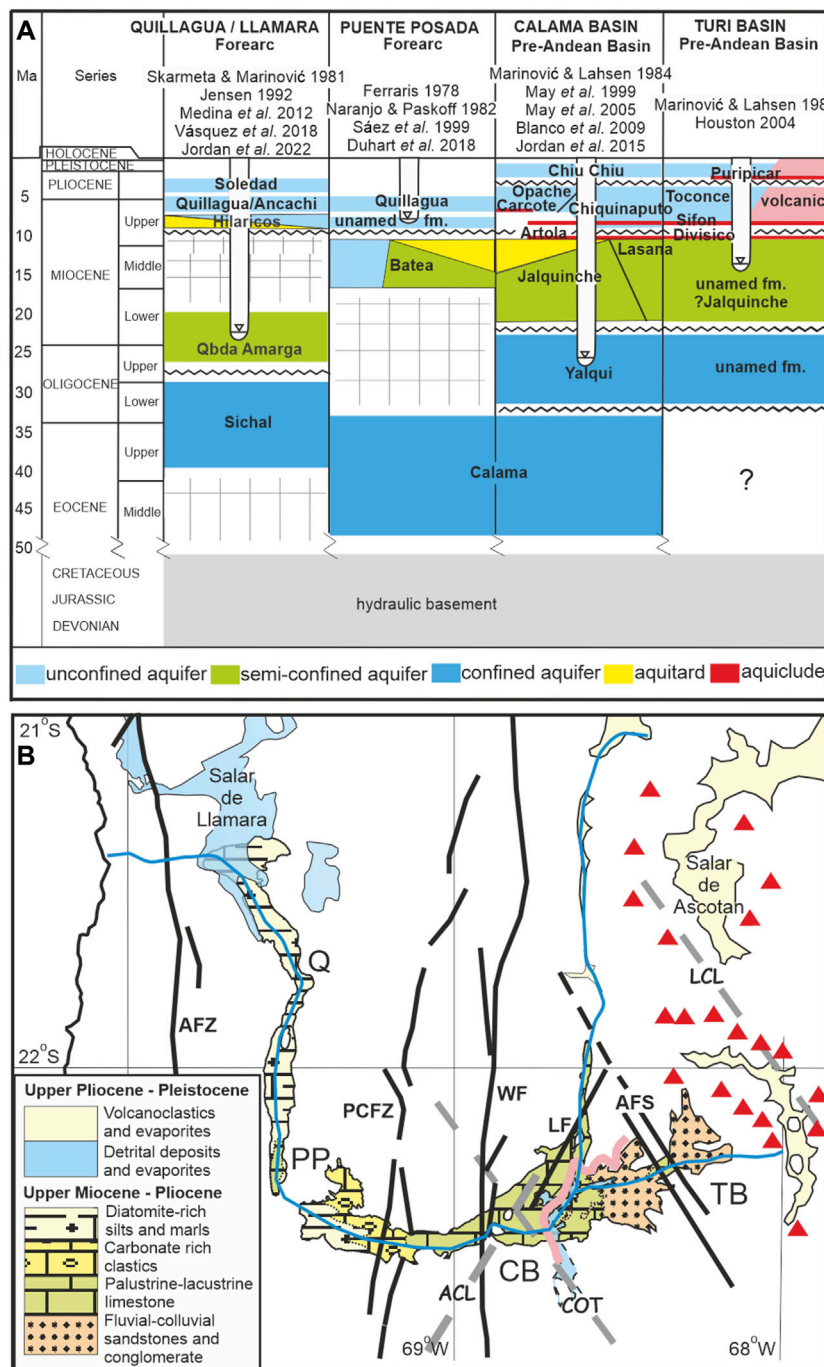


FIGURE 2

Catchment geology. (A) schematic hydrostratigraphic chart for major forearc and Pre-Andean basins in the Río Loa catchment. The aquifer conditions for Quillagua-Llamara and Puente Posada are based on outcrop lithology, geological mapping and inferred hydrogeological conditions. The Calama and Turi Basins are based on geological mapping, drilling, geophysical logging and well test data. Generalized river incision in relation to formations for each area is shown. Published sources are given for each basin. (B) lithology and structure of formations hosting the upper, phreatic aquifers within the surface water catchment of the Ríos Loa and Salado. Q- Quillagua, PP- Puente Posada, CB- Calama Basin, TB- Turi Basin. AFZ- Atacama Fault Zone, PCFZ- Pre-Cordillera Fault Zone, WF- West Fissure Fault Zone, LF- Loa Fault, AFS- Ayquina Fault System. ACL- Antofagasta-Calama Lineament, COT- Calama-Olcapato-El Toro Lineament, LCL- Lipez-Coranzuli Lineament. Pink line- Calama Basin monocline. Red triangles-volcanoes.

groundwater resources within its catchment. The resource is now in danger of being so exploited as to cease functioning at some point in the future. Sustainable management of these resources needs to be based on detailed knowledge of the system as a hydrological entity. Whilst considerable attention has been paid to the groundwater

resources of the Río Loa catchment, little has been paid to the surface water system, except for the pioneering isotopic work of Magaritz et al. (1989), Aravena and Suzuki (1990) and Aravena (1995).

Surface water runoff is initiated by precipitation, but over 90% of annual precipitation in the catchment of the Río Loa occurs at high

altitude in the summer months of December to February (DJF) (Garreaud et al., 2009; Espinoza et al., 2020; Arias et al., 2021; Houston and Latorre, 2022). The river is maintained throughout the rest of the year by interflow and baseflow which originate as transient release from the vadose zone and long-term discharge from groundwater respectively (Horton, 1933; Barnes, 1939; Rorabaugh, 1964). For any gauging station, only active aquifer storage above the elevation of the gauging station contributes to baseflow; once the groundwater gradient decays to this putative level, flow ceases. However, this does not preclude deeper groundwater entering the hydrological cycle, where topographic and flow gradients are steep (Tóth, 2009; Frisbee et al., 2017; Somers and McKenzie, 2020), nor the possibility that the hydraulic basement as currently envisaged (Figure 2) (Naranjo and Pascoff et al., 1982; Herrera et al., 2021) may be permeable on long timescales, as a result of diffusivities greater than zero, and as changes in baselevel, gradients or recharge rates occur (Manning and Ingebritsen, 1999; Ingebritsen and Manning, 2002; Diamond et al., 2018). Crucially, it is hypothesized that lithospheric sources such as geothermal, magma volatile release and/or subduction dehydration may enter the hydrological cycle associated with arc volcanism (Aravena and Suzuki, 1990; Godfrey et al., 2019; Godfrey et al., 2021). Several aquifers have been identified within the catchment (Figure 2): high altitude intra-arc, structurally and volcanically controlled aquifers (Houston, 2009; Urrutia et al., 2019), Pre-Andean Calama and Turi Basin volcano-sedimentary aquifers at 2,300–3,200 m (Houston, 2004; Jordan et al., 2015), and forearc hosted aquifers of the Central Depression (JICA, 1995; Houston et al., 2001; Rojas et al., 2010; Samuel et al., 2019; Viguier et al., 2019; Jordan et al., 2022).

Additionally, several recent studies (Jordan et al., 2002; Corenthal, 2016; Munk et al., 2018; Moran et al., 2019; Boutt et al., 2021) have suggested that so-called orogenic groundwater (here termed far-field) flow that is sourced from beyond the surface water catchment boundaries, contributes significant fluxes to both surface and groundwater along the western slope of the Andes. The most extensively reported example is to the south, in the Salar de Atacama where both the water and salt fluxes within the catchment appear to be out of balance unless sources outside the catchment are taken into consideration (Moran et al., 2019; Boutt et al., 2021). To the north, Magaritz et al. (1990), Aravena (1995), Jayne et al. (2016) and Alvarez-Campos, et al. (2022) have all suggested that a proportion of the groundwater in the Pampa Tamarugal (Central Depression) originates from the high Andes as infiltrating surface water, transmitted via deep seated fissures open to groundwater flow. Elsewhere, smaller scale cross-catchment boundary flow has been widely reported (Anderson et al., 2002; Montgomery et al., 2003; Houston, 2006c; Rissmann et al., 2015).

The present study is based on a field program during 1999–2001 that measured twenty two surface water flows, and seven springs at different times of the year, at selected locations throughout the whole catchment, concurrently obtaining water samples for major ion and isotope analysis. Daily precipitation and river flow data for the period 1976–2001 were obtained from the Dirección General de Aguas (DGA) for three key locations, in order to place the study data in context, whilst groundwater and geothermal data from the literature are also used to provide background and are referenced in the text. The study integrates

physical, chemical and isotopic aspects in order to explain the hydraulic and hydrogeochemical processes throughout the catchment. In particular, the origins of the system in the volcanic arc are examined in relation to lithospheric processes. The results have wider implications for fluvial activity in arid regions, subduction zones worldwide, and specifically for the sustainable management of water resources in northern Chile.

2 The Río Loa catchment

2.1 Morphological development

These hydrological systems have their origin in the uplift of the Andes. Figure 1A is a DEM of the catchment showing its major morphological features. Shallow slopes of $<2^\circ$ signify basins with volcano-sedimentary infill hosting the major aquifers throughout the catchment, whilst slopes of $2\text{--}4^\circ$ are generally indicative of colluvium and alluvial fans where significant recharge takes place under favourable conditions (Houston, 2002). The thalweg of the Río Loa is around 450 km long from its catchment boundary (maximum elevation $\sim 6,000$ m) to the ocean encompassing approximately 33,570 km². The river presents three segments, each with coherent gradients reflecting successive phases of tectonic uplift (Hoke et al., 2007). At the upper bound of each segment lie three deeply incised canyons, 110–170 m deep in the Western Cordillera, 160–190 m deep through the Pre-Cordillera and 450–490 m deep through the Coastal Range. Each canyon ends with a significant knickpoint that appears to have stalled in its upstream migration where it encounters resistant bedrock. The upstream lip of the gorges is the effective base level for active groundwater storage in the basins above, which are up to 1 km or more deeper than the canyon lip (Jordan et al., 2015; Jordan et al., 2022), suggesting that there may be considerable stagnant or slowly overturning storage within them. Localised dewatering of these aquifers orthogonal to the river occurred during incision distorting adjacent groundwater flow nets (Houston, 2006c).

The forearc and Pre-Andean basins were infilled with clastic sediments, together with repeated pyroclastic deposits, and progressively overlain by carbonate, sulphate and halite evaporites between the Eocene and Late Miocene (De Silva, 1989; Lamb, 2016; Garzzone et al., 2017; Horton, 2018; Jordan et al., 2022). The Calama Basin was largely endoreic during this period (May et al., 1999; Blanco et al., 2003; Mpodozis et al., 2005), but beginning 10–7 Ma, sedimentation spilled over the Pre-Cordillera through the Calama Gap to the Central Depression with deposition of the Opache Formation (May et al., 1999; May et al., 2005; Hoke et al., 2007; Jordan et al., 2010; Jordan et al., 2015). However, surface water flow beyond Calama to the Central Depression was limited, as demonstrated by shallow gradients ($<1^\circ$) and transient ponding in the Calama gap (Houston et al., 2001; Jordan et al., 2010; de Wet et al., 2015; de Wet et al., 2020). Uplift of the Western Cordillera due to tectonic activity and tilting took place during the Middle Miocene through the Pliocene (Hartley and Evenstar, 2010; Jordan et al., 2010; Evenstar et al., 2016) leading to incision of the Río Toconce on the western slope of the Cordillera between 3.9 and 1.1 Ma (Houston, 2006c) and the paired Ríos Loa and San Salvador as marginal drainage channels through the structural gap in the

Pre-Cordillera and fully connecting the Calama Basin with the forearc hydraulically post ca. 3 Ma (May et al., 1999; Hartley and Evenstar, 2010).

The Central Depression between Quillagua and the Salar de Llamara was also endoreic from the Eocene, with a significant Plio-Pleistocene evaporite sequence overlying lacustrine carbonates and clastics. Accommodation space in the basin was filled by this sequence, which, coupled with tectonic activity caused breaching of the Coastal Range at its lowest point allowing the Río Loa to incise the canyon that led to a new (oceanic) baselevel after ca. 0.3–0.2 Ma (Sáez et al., 1999; Sáez et al., 2012; Mohren et al., 2020; Jordan et al., 2022).

2.2 Geology and aquifers

The geology of these basins has been studied extensively (Ferraris, 1978; Skarmeta and Marinović, 1981; Naranjo and Pascoff, 1982; Marinović and Lahsen, 1984; Jensen, 1992; Sáez et al., 1992; Medina et al., 2012; Duhart et al., 2018; Vásquez et al., 2018; May et al., 1999; Houston, 2004; May et al., 2005; Blanco et al., 2009; Jordan et al., 2015; Jordan et al., 2022) so that a hydrostratigraphic chart can be presented (Figure 2A), in addition to a sketch map of the lithology hosting the upper, phreatic aquifers of the catchment (Figure 2B). Here the geology is only briefly reviewed with respect to the main aquifers.

At high elevations volcanic edifices and ignimbrite sheets of Miocene to Pleistocene age have steep slopes giving rise to rapid runoff as well as infiltration into a series of perched aquifers consisting of unconsolidated ashes, tuffs and blocky lava interbeds. Within the Western Cordillera a number of aerielly small intra-arc sedimentary basins exist at elevations between 3,700 and 4,500 m. Despite their apparently limited size these basins and associated porous volcanic edifices represent intra-arc aquifers which are of particular interest since they receive significant recharge under present day conditions (e.g., Linzor Basin - Houston, 2009), and are a major source of supply for nearby copper mines (e.g., San Pedro-Inacaliri Basin).

Mesozoic rocks with low matrix permeability dominate the Pre-Cordillera. Between the high Cordillera and Pre-Cordillera a series of moderately sized Pre-Andean basins occur: the Calama and Turi Basins. Houston (2004) identified upper and lower aquifers in the Calama Basin separated by an intermediate aquiclude-aquitard, and recent studies have confirmed this (Blanco and Tomlinson, 2009; Tomlinson et al., 2010; Jordan et al., 2015; Herrera et al., 2021). The upper aquifer in the Turi and Calama Basins is hosted by the Toconce, Chiquinaputo and Opache Formations, largely fluvio-clastic and palustrine-lacustrine carbonate sediments (Figure 2). The lower aquifer in the Calama Basin is hosted by the coarse to fine-grained clastic sediments of the Jalquinche, Lasana, Yalqui and possibly the Calama Formations, and by an unnamed formation (assumed to be an extension of the Jalquinche Formation) into the Turi Basin. The aquitard separating the upper and lower aquifers in the Calama Basin is a mixture of welded ignimbrite (principally the Sifon Ignimbrite) and clay-rich facies of the Jalquinche Formation (Houston, 2004; Jordan et al., 2015; Herrera et al., 2021).

Between the Pre-Cordillera and Coastal Range lies the extensive Central Depression (Pampa Tamarugal) with several, serially connected basins rising northward (and hence draining south toward the Río Loa) from 700 to 1,300 m, as a result of tectonic activity on cross-strike faults (JICA, 1995; Rojas et al., 2010; Samuel et al., 2019; Viguier et al., 2019; Jordan et al., 2022). The Quillagua Formation, largely comprised of palustrine carbonates together with diatom-rich silts and marls is equivalent to the upper aquifer of the Calama Basin, whereas the Quebrada Amarga Formation comprised of carbonates and clastic sediments (Sáez et al., 1999; Vásquez et al., 2018; Jordan et al., 2022) represents a semi-confined lower aquifer in the vicinity of Quillagua-Llamara, becoming unconfined in the vicinity of the Río Loa incised valley.

A number of structures conceivably impact groundwater, and potentially surface water flow by extrapolation (Figure 2B). A series of long-lived north-south along-strike faults, at various times in their history normal, reverse, and strike-slip occur sequentially from west to east: the Atacama Fault Zone bounding the fore-arc basins (Brown et al., 1993), the Pre-Cordillera Fault and the West Fissure, bounding the Pre-Andean Basins (Reutter et al., 1993; López et al., 2020), the Loa Fault (Jordan et al., 2015) and the Ayquina Fault system bounding the Turi Basin (Houston, 2004). Three deep seated, crustal lineaments cross the Calama Basin obliquely: The Antofagasta-Calama (NE-SW), and both the Calama-Olcapato-El Toro and the Lipez-Coranzuli lineaments (NW-SE) (Palacios et al., 2007; Lanza et al., 2013; Norini et al., 2013; Tibaldi et al., 2017). Finally, the Chiu Chiu monocline, a sinuous monocline dividing the northwest part of the Calama Basin from the southeast may also affect groundwater flow (Blanco and Tomlinson, 2009; Jordan et al., 2015).

2.3 Climate

Convective activity generated by the South American Summer Monsoon (SASM) brings low-latitude summer precipitation to the basin, while the Southern Hemisphere Westerlies (SHW) bring winter precipitation from high latitudes. Between these systems lies the Andean Dry Diagonal (ADD), a zone of minimal precipitation at the core of the Atacama Desert (Garreaud et al., 2003; Arias et al., 2021; Houston and Latorre, 2022). Precipitation is strongly influenced by the Andes which create a rainshadow on their western slopes: 3.5 mm at Calama (2,300 m), compared with ~120 mm/a at 4,000 m (Houston and Hartley, 2003). The Río Loa catchment lies at the core of the Atacama Desert, largely to the north of the ADD where ca. 90% of rainfall occurs in the summer months (DJF) compared with >90% south of the ADD during winter (AMJJAS) (Garreaud et al., 2003; Espinoza et al., 2020; Arias et al., 2021; Houston and Latorre, 2022; Valdivielso et al., 2020). Although it is recognized that winter precipitation occurring as snow is often under recorded (Vuille and Ammann, 1997).

High-intensity long-duration convective precipitation is required to generate extreme flood runoff and groundwater recharge events, which occurs sporadically over the Western Cordillera and Pre-Cordillera (Houston, 2005; Houston, 2006b; Poveda et al., 2020). Such extreme events are augmented by quasi-

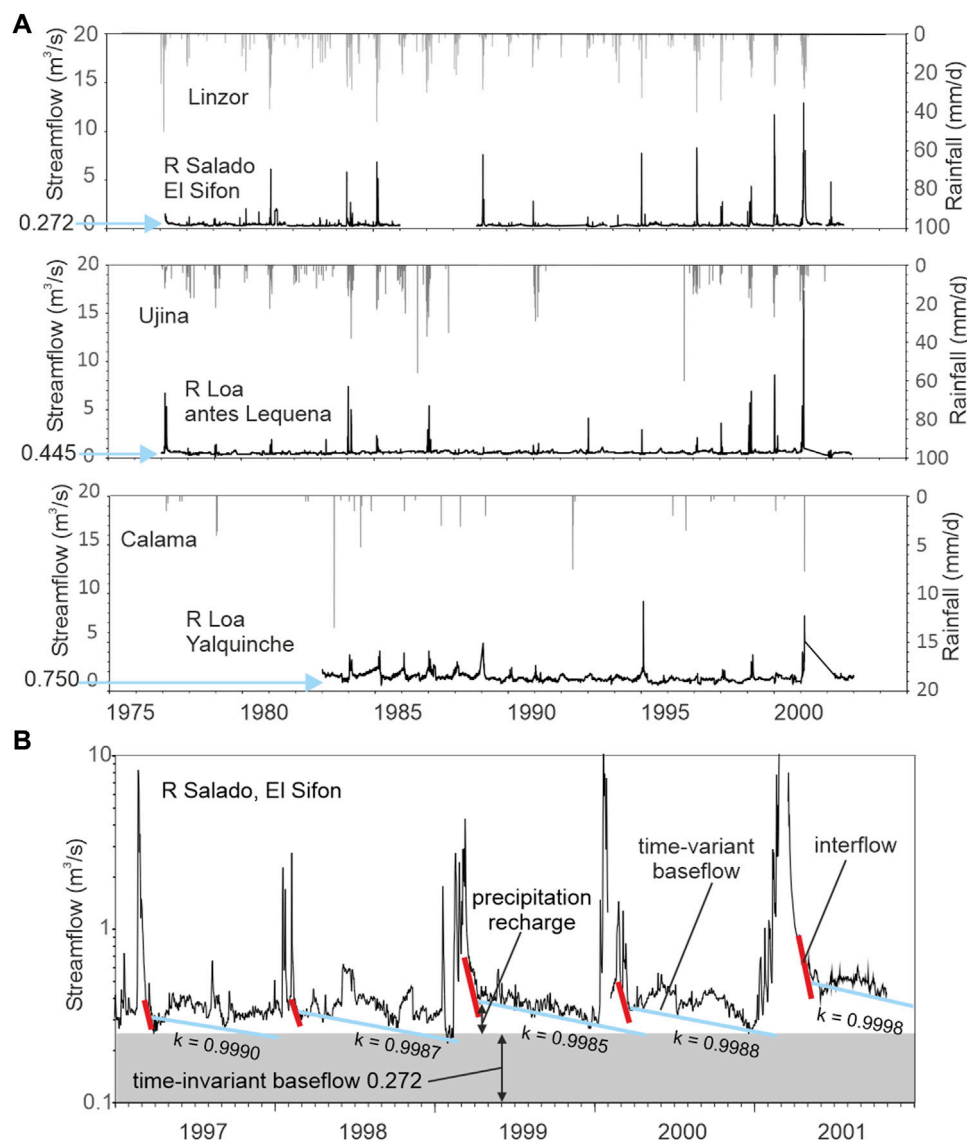


FIGURE 3

Flow time series. (A) stream hydrographs and precipitation at three key locations within the Loa catchment, with time-invariant flow rate arrowed. (B) recession analysis for Río Salado at El Sifon (locality 17).

periodic circulation modes: El Niño-Southern Oscillation, Atlantic sea surface temperature, Pacific Decadal Oscillation, and the Madden Julian Oscillation (Lenters and Cook, 1997; Takahashi et al., 2011; Boers et al., 2015; Valdés-Pineda, 2018; Sun et al., 2019; Espinoza et al., 2020; Vuille et al., 2000).

Of particular importance to past groundwater recharge are the wetter precipitation episodes that occurred during the Holocene and Late Pleistocene (de Porras et al., 2021; González-Pinilla et al., 2021). Wetter periods tend to have recurred at intervals of 10^2 – 10^3 years, although not always with the same intensity. The Central Andean Pluvial Event (CAPE; 15.9–7.5 ka BP) led to widespread perennial discharge in what are now ephemeral channels (Latorre et al., 2002; Houston, 2005; Nester et al., 2007; Gayo et al., 2012), and likely contributed to contemporaneous groundwater recharge events, the latest arguably in the Late Holocene (5.0–4.6, 3.2–2.1 and 1.4–0.7 ka BP) (Tully et al., 2019; González-Panilla et al., 2021).

3 Hydrology

3.1 Flow regime

The perennial river network is shown in Figure 1B. Three principal high altitude subcatchments; the upper Loa, San Pedro and Salado are all fed from aquifers during the dry season. A middle section transfers water from these catchments through the gap in the Pre-Cordillera, from where the lowest section crosses the hyper-arid forearc basin, finally to discharge into the Pacific Ocean. A number of tributaries are present, especially in the Salado catchment, as well as minor springs throughout which are inferred to represent bank storage return water (see Supplementary Material S1).

Using data from the Chilean national catchment dataset: CAMELS-CR2, (Alvarez-Garretón, et al., 2018), daily rainfall and stream flows for three key stations are plotted in Figure 3A for the

TABLE 1 Catchment characteristics, estimated recharge and aquifer properties for the middle and upper Ríos Loa and Salado derived from recession analysis of baseflow.

	Salado El Sifon	Loa antes Lequena	Calama Yalquinche
Latitude S	22.28	21.66	22.45
Longitude W	68.32	68.66	68.88
Gauging sta location (see Figure 4)	17	12	7–9
Catchment area (A - km ²)	770	2010	9,770
Perennial stream lengths (L - km)	61	69	208
Gauging station elevation (H - m a.s.l.)	3,031	3,314	2,300
Low flow threshold (m ³ /s)†	0.272	0.445	0.750
Time variant flow (m ³ /s)	0.046	0.0438	0.138
Evapotranspiration losses (m ³ /s)*	0.044	0.880	0.880
Baseflow (m ³ /s)	0.362	1.369	1.768
Annual baseflow per unit area (m ³ /a/km ²)	1.48 × 10 ⁴	0.96 × 10 ⁴	0.36 × 10 ⁴
Recession constant average (k - days ⁻¹)	0.9990	0.9994	0.9988
End dry season active storage remaining (m ³)	11.5 × 10 ⁶	16.8 × 10 ⁶	32.4 × 10 ⁶
Annual recharge to catchment (mm/a; 1σ)	14.8 ± 1.5	9.6 ± 5.1	3.5 ± 0.28
Estimated recharge area (km ²)*	490	1,170	3,614
Estimated recharge area as percent of A	64%	58%	37%
Mean annual recharge to aquifers (mm/a)	23.3	16.4	9.6
Max diffusivity = Kb/Sy (m ² /s)	1,509	1930	7,838

† time-invariant flow.

* see [Supplementary Material](#).

** based on suitable lithologies from geological maps.

years 1975 through 2002, and their details are given in [Table 1](#). The rainfall station at Linzor for the Río Salado (at El Sifon), and Ujina for the Río Loa (above Lequena) are located near the respective upper catchment boundaries, at some distance from the stream gauging site but illustrative of catchment precipitation, whereas that for Yalquinche (Calama) is adjacent to the gauging site. Low flow for these stations is defined as the lowest daily flow recorded at the end of the dry season (usually November), and baseflow is defined as all flow that occurs after direct runoff and interflow have ceased and before the next flood.

Summer rainfall events give rise to flood peaks with short lag times in all stations, indicating a rapidly responding flash flood regime typical of arid environments (see [Supplementary Material S2](#)). Lequena and El Sifon have flash flows correlated with their respective rainfall stations, but it is noteworthy that Calama flood events are mainly out of phase with local precipitation demonstrating that summer precipitation-runoff events in the Western Cordillera influence the river throughout its course ([Houston and Hartley, 2003](#); [Houston, 2006b](#); [Houston and Latorre, 2022](#)). The flood peak is always short-lived, usually no more than a few days after the rainfall peak, although there may be more than one event per season. Thereafter, interflow, the release of water taken into bank storage during intense rainfall and flood flow, dominates, and depending on the magnitude and intensity of the rainfall event, normally lasts no more than 1–2 months. After bank storage has been depleted the remainder of the dry season flow is supported by baseflow. During

this period frequent low-amplitude, low-frequency increases in flow occur during the winter months April to September. The cause of these small (<0.1 m³/s) increases in flow are postulated to be due to one or more of the following: a) winter precipitation including snowmelt, b) reduced winter evaporation, or c) human intervention. The data to support a) or b) of these options is inconclusive. Human intervention (c) in the form of irrigation takeoff and return, as well as abstraction and reservoir release on a daily basis are a mostly unknown and unrecorded quantitative feature of streamflow. Nevertheless, [Figure 3B](#) shows that baseflow and recession can still be clearly identified.

During the period 1977–2002 low flows never drop below a threshold specific to each gauging station ([Figure 3](#); [Table 1](#)), and the recession is asymptotic to the low flow threshold value and never to zero. The threshold is stable over time arguing against it being a precipitation related source which would be variable year-on-year. This time-invariant component of baseflow is theorized to have its source within the lithosphere from several possible causes: a) slab dehydration ([Ingebritsen and Manning, 2002](#)), b) magma volatile exsolution (e.g., [Urann et al., 2022](#)), c) hydrothermal discharge ([Giggenbach, 1992](#)), d) deep recirculation of meteoric water ([Diamond et al., 2018](#)), or e) far-field (extra catchment) recharge ([Boutt et al., 2021](#)). These possibilities are explored further below.

Based on the lowest flows in the upper reaches of the Loa and Salado subcatchments (localities 17 and 12), the combined time-

invariant flow is 0.717 m³/s, only 0.03 m³/s (4%) less than that in the Loa at Calama (between localities 7 and 9). The difference may be accounted for by additions from the Río San Pedro, a left bank tributary of the Río Loa joining between localities 11 and 12, which has average low flows of <0.1 m³/s at the confluence. Critically, the lack of *additional* flow in the Pre-Andean basins signifies that the upper Ríos Loa and Salado supply virtually all low flow at Calama.

Data from October 1916 reported by Jordan et al. (2015) indicate that in the era before large scale abstraction took place, baseflow was 1.0–2.5 m³/s greater throughout the middle Loa (Calama Basin), and possibly as much as 3 m³/s greater in the upper Loa basin.

3.2 Recession analysis

Analysis of the recession curve allows for the estimation of groundwater storage depletion, or contribution to baseflow over time. Baseflow is derived from active storage within an aquifer and is controlled by the physical properties of the aquifers (Szilagyi et al., 1998; Wittenberg, 1999; Troch et al., 2013). Analysis of the recession curve assumes no significant anthropogenic interventions such as reservoirs, abstraction or return flows (Singh and Stall, 1971; Sujono et al., 2004; Bloomfield et al., 2011; Yao et al., 2021). Such interferences do occur at several locations on the Ríos Loa and Salado (Figure 1B), although during the period of analysis (1977–2002) the slope of the recession limbs remain virtually constant for each station, suggesting that artificial regulation is either short-lived or near-constant in time. With the possible exceptions of the small variations as noted above, a simple tripartite division of the receding limb into flood runoff, interflow, and groundwater baseflow can be made. For the purpose of recession analysis, the storage reservoir is assumed to be a single horizontal, uniform, homogeneous aquifer with no bedrock leakage (Hall, 1968; Tallaksen, 1995; Troch et al., 2013). Since the recession occurs over a long period dry season (>280 days) the initial critical time (change from interflow to baseflow) becomes less important (Anderson and Burt, 1980; Szilagyi et al., 1998; Sujono et al., 2004) and the recession in its simplest form (Barnes, 1939) is then given by:

$$Q_t = Q_0 k^t \quad (1)$$

where Q_0 is the initial flow, Q_t the flow at time t after the initial flow and before any further flood flow, and k is the recession constant. By integration this leads to the storage equation where S (the volume remaining in active storage after time t):

$$S = - (Q_t - Q_0) / k \quad (2)$$

Furthermore, at long times the aquifer hydraulic diffusivity (D) can be calculated from the recession constant thus:

$$D = 4L^2 / \pi^2 k \quad (3)$$

where L is the length of the perennial river from the gauging station to the divide and k is the recession constant (Rorabaugh, 1964; Szilagyi et al., 1998). The diffusivity (D) of the source aquifer is a function of its properties:

$$D = Kb / Sy \quad (4)$$

where K is the hydraulic conductivity, b the aquifer thickness and Sy is the effective porosity (more correctly the specific yield). Kb is also

equal to T , the transmissivity. Finally, the magnitude of the year-on-year displacement of the recession curve at the moment when interflow ceases and baseflow initiates is equivalent to the annual recharge of the storage reservoir (Meyboom, 1961; Szilagyi et al., 1998; Chen and Lee, 2003).

Evapotranspiration losses are additional to measured baseflow. Above 3,000 m widespread Puna and high Andean vegetation belts reduce infiltration and enhance evapotranspiration, as do spring-fed wetlands (Vilagrán et al., 1981; Houston, 2006a; Suárez et al., 2023). In the middle and lower reaches, evaporation is limited to in-channel areas, and transpiration to riparian vegetation. Estimated evaporation rates based on elevation (Houston, 2006a) and isotopic fractionation provide an estimate (see Supplementary Material S3) that varies from 0.04 to 0.12 m³/s in the upper catchments and 0.21 m³/s in the Calama Basin.

Throughout the catchments, the respective hydrographs show no changing impact from abstraction during the period of analysis, so that no allowance for abstractions is made in the recession analysis.

The Río Salado at El Sifon is used as an example of the technique (Figure 3B) which is then applied to all three streamflow stations (Table 1). When plotted in semi-logarithmic form baseflow recession yields a straight line, with the slope equal to the recession constant (k). Single, near-parallel late-stage recession curves support the concept of an ideal single linear reservoir (aquifer) with annual replenishment. However, given the rather noisy data (see above), a graphical technique for the derivation of the recession constant k , and the moment of baseflow initiation has been favored (Szilagyi et al., 1998; Sujono et al., 2004; Stoelzle et al., 2020).

Mean values of k for each subcatchment are given in Table 1 and vary from 0.9988 through 0.9994 per day. Such consistently high values of k are indicative of slow recession from large active storage reservoirs. Unusually, each year's recession decays to the same flow rate, and this is true for all three gauging stations. Typically, wet years should end on higher flows and *vice versa*. This limiting flow may be labelled as time-invariant flow, whilst all baseflow above this rate is considered time-variant. Mean time-variable baseflow for the upper Ríos Loa and Salado is 0.04 and 0.05 m³/s respectively, whilst the time-invariant components (baseflow minus time-variant flow) averages 0.57 and 0.32 m³/s. Unit baseflows are 0.96×10^4 m³/a/km² for the upper Río Loa and 1.48×10^4 m³/a/km² for the Salado. Unit baseflow in the Río Loa at Calama (0.36 m³/a/km²) is significantly lower because it is generated in only a small proportion of the total catchment (above ~3,000 m).

Active storage at year (dry season) end is $\sim 28 \times 10^6$ m³ for the upper catchments combined, compared with 32×10^6 m³ for the whole catchment at Calama, indicating 88% is derived from intra-arc aquifers above ~3,000 m. This large buffer against stream desiccation in the dry season, is interpreted as the reason for the perennial nature of the Loa-Salado river system.

Diffusivity is high for all active storage reservoirs, implying that permeability will be high, whereas specific yield is likely to be low suggesting semi-confined conditions (see Supplementary Material S4), and indicating coarse clastic or pyroclastic material possibly with significant fracture flow.

Annual precipitation recharge for each subcatchment based on the recession curve displacement method gives values between

TABLE 2 Instantaneous water budget for the Río Loa-Salado transect during baseflow and interflow conditions.

Fig 1 ref #	Location	Distance from ocean	Lat	Long	Altitude	Measured flow October 1999	Cumulative tributary flow	Cumulative licensed abstraction*	Adjusted flow**	Gain/loss	Gain/loss per km
		km									
Baseflow October 1999											
	sea	0.0	-21.43	-70.06	0	0.00	1.23	0.40	-0.83	-0.70	-466.67
1	Loa mar	1.5	-21.43	-70.04	31	0.70	1.23	0.40	-0.13	0.10	1.54
	Quillagua bridge	66.5	-21.64	-69.55	791	0.60	1.23	0.40	-0.23	-0.05	-4.73
2	Quillagua sta	77.1	-21.67	-69.54	804	0.65	1.23	0.40	-0.18	0.00	0.00
3	Cruces Las Torres	144.7	-22.28	-69.97	1,158	0.65	1.23	0.40	-0.18	-0.01	-0.63
	Chacance	160.5	-22.40	-69.51	1,100	0.66	1.23	0.40	-0.17	0.00	0.00
4	Chacance antes San Salvador	160.6	-22.40	-69.52	1,185	0.47	1.04	0.40	-0.17	0.02	0.31
7	Cascad	226.0	-22.51	-68.98	2,180	0.45	1.04	0.40	-0.19	-0.43	-10.18
9	Angostura	268.2	-22.46	-68.73	2,460	0.88	1.04	0.40	0.24	-0.10	-7.28
	Loa confluence Salado	282.0	-22.27	-68.63	2,400	0.98	1.04	0.40	0.34	0.00	0.00
	Salado antes Loa	282.1	-21.95	-68.61	2,500	0.48	0.54	0.40	0.34	0.00	0.00
16	Salado Chiu Chiu bridge	293.6	-22.33	-68.56	2,555	0.48	0.54	0.40	0.34	-0.21	-7.95
17	El Sifon	320.0	-22.28	-68.32	2,890	0.69	0.54	0.40	0.55	0.00	0.00
	Salado after Caspana	329.0	-22.27	-68.26	3,040	0.69	0.54	0.40	0.55	0.00	0.00
	Salado antes Caspana	330.0	-22.28	-68.24	3,085	0.40	0.25	0.40	0.55	0.02	7.58
	Salado after Toconce	332.6	-22.28	-68.21	3,118	0.15	0.02	0.40	0.53	0.03	7.10
	Toconce confluence Salado	336.9	-22.27	-68.21	3,141	0.10	0.00	0.40	0.50	0.05	15.94
18	Toconce	340.0	-22.27	-68.15	3,300	0.05	0.00	0.40	0.45	0.05	23.32
	Toconce antes represa	342.1	-22.28	-68.14	3,449	0.35	0.00	0.05	0.40	-0.40	-47.35

(Continued on following page)

TABLE 2 (Continued) Instantaneous water budget for the Río Loa-Salado transect during baseflow and interflow conditions.

Fig 1 ref #	Location	Distance from ocean	Lat	Long	Altitude	Measured flow October 1999	Cumulative tributary flow	Cumulative licensed abstraction*	Adjusted flow**	Gain/loss	Gain/loss per km
		km				m ³ /s					
	Toconce ford	350.6	-22.24	-68.05	3,988	0.75	0.00	0.05	0.80	0.37	50.05
19	Linzor	358.0	-22.23	-68.03	4,050	0.38	0.00	0.05	0.43	0.43	58.17
	source	365.4	-22.24	-67.98	4,360	0	0.00	0	0	0	0
Interflow March 2000											
	sea	0.0	-21.43	-70.06	0	0.00	1.60	0.40	-1.20	-1.10	-733.33
1	Loa mar	1.5	-21.43	-70.04	31	1.10	1.60	0.40	-0.10	-0.05	-0.77
	Quillagua bridge	66.5	-21.64	-69.55	791	1.15	1.60	0.40	-0.05	-0.09	-8.52
2	Quillagua sta	77.1	-21.67	-69.54	804	1.24	1.60	0.40	0.04	-0.06	-0.89
3	Cruces Las Torres	144.7	-22.28	-69.97	1,158	1.30	1.60	0.40	0.10	-0.35	-22.10
	Chacance	160.5	-22.40	-69.51	1,100	1.65	1.60	0.40	0.45	0.00	0.00
4	Chacance antes San Salvador	160.6	-22.40	-69.52	1,185	0.55	0.50	0.40	0.45	-1.65	-25.32
7	Cascad	226.0	-22.51	-68.98	2,180	2.21	0.50	0.40	2.11	1.11	26.16
9	Angostura	268.2	-22.46	-68.73	2,460	1.10	0.50	0.40	1.00	0.15	10.93
	Loa confluence Salado	282.0	-22.27	-68.63	2,400	0.95	0.50	0.40	0.85	0.00	0.00
	Salado antes Loa	282.1	-21.95	-68.61	2,500	0.65	0.20	0.40	0.85	0.26	22.59
16	Salado Chiu Chiu bridge	293.6	-22.33	-68.56	2,555	0.60	0.41	0.40	0.59	0.05	1.89
17	El Sifon	320.0	-22.28	-68.32	2,890	0.55	0.41	0.40	0.54	0.25	27.68
	Salado after Caspana	329.0	-22.27	-68.26	3,040	0.30	0.41	0.40	0.29	-0.29	-290.00
	Salado antes Caspana	330.0	-22.28	-68.24	3,085	0.30	0.12	0.40	0.58	0.24	90.91
	Salado after Toconce	332.6	-22.28	-68.21	3,118	0.01	0.07	0.40	0.34	-0.07	-16.57
	Toconce confluence Salado	336.9	-22.27	-68.21	3,141	0.01	0.00	0.40	0.41	-0.37	-117.98

(Continued on following page)

TABLE 2 (Continued) Instantaneous water budget for the Rio Loa-Salado transect during baseflow and interflow conditions.

Fig 1 ref #	Location	Distance from ocean	Lat	Long	Altitude	Measured flow October 1999	Cumulative tributary flow	Cumulative licensed abstraction*	Adjusted flow**	Gain/loss	Gain/loss per km
		km			m a.s.l.	m ³ /s	m ³ /s	m ³ /s	m ³ /s	m ³ /s	m ³ /s/km ×10 ³
18	Toconce	340.0	-22.27	-68.15	3,300	0.38	0.00	0.40	0.78	-0.07	-32.65
	Toconce antes represa	342.1	-22.28	-68.14	3,449	0.80	0.00	0.05	0.85	-0.18	-21.31
	Toconce ford	350.6	-22.24	-68.05	3,988	0.98	0.00	0.05	1.03	0.37	49.38
19	Linzor	358.0	-22.23	-68.03	4,050	0.62	0.00	0.05	0.67	0.67	89.96
	source	365.4	-22.24	-67.98	4,360	0	0.00	0	0	0	0

* only major abstractions accounted for.

** = measured flow - tributary flow + abstraction.

† Jordan et al., 2015.

10 and 15 mm/a above 3,000 m, and less than 5 mm/a at 2,300 m (Table 1). These estimates are based on total areas, yet it is probable that not all areas allow infiltration to the water table. Based on assumptions regarding suitable lithologies that might allow infiltration applied to existing geological maps (Marinović and Lahsen, 1984), conjectured recharge areas for each subcatchment are given in Table 1, which lead to actual precipitation recharge rates of 16–23 mm/a above 3,000 m.

3.3 Instantaneous flow transect

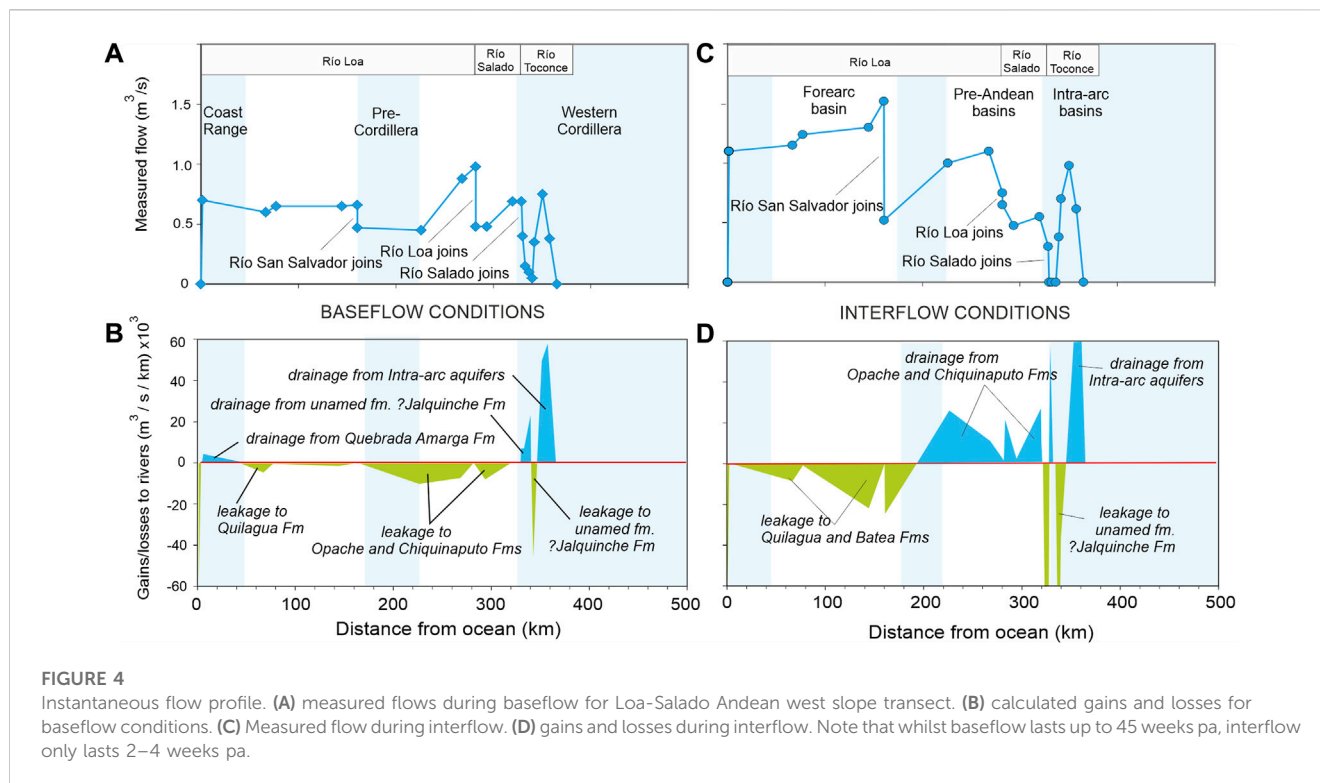
During October 1999 stream flows were measured throughout the Loa and Salado Basins, with the objective of identifying and quantifying gaining and losing reaches that might indicate transfers from or to groundwater sources respectively. Temporary gauging sites were located along an east-west alignment from the catchment boundary in the Western Cordillera (Río Toconce), then due west along the Río Salado and Río Loa to the point where the latter eventually turns north and then west to the ocean. This section was chosen to give a typical hydraulic profile of the western Andean slope but does not give the full flow conditions for the whole catchment. Measurements were made using a float and the velocity-area method (Dingman, 1993) on suitable straight and uniform reaches of ~3 m. Three to five repeat measurements at each site suggest that errors were <7%. Although these measurements took 5 days to cover the whole catchment, the data effectively give an instantaneous picture of the surface water balance. The measurement sites are located in Figure 1B and the results are shown in Table 2 and Figure 4. In order to discount tributary inflows to and licensed abstractions from the transect analysis, the adjusted flow at each site was calculated as:

$$Q_A = Q_O - Q_T + Q_L \quad (5)$$

where Q_A is the adjusted flow, Q_O is the measured flow, Q_T is the tributary flow which accounts for off-transect surface water gains, and Q_L is the licensed abstraction on-transect. There are three tributaries whose contributions need to be discounted (Figure 4), as well as licensed abstractions at Linzor (0.05 m³/s), and Toconce (0.35 m³/s) that need to be accounted. At several points along the transect, notably Toconce, Ayquina, Calama and Quillagua un-monitored agricultural takeoffs exist. These are not included in the analysis since a) their magnitude is not known with accuracy, and b) much of the water is returned via small-scale canalization. A repeat flow inventory was carried out in March 2000, when the hydrographs show that the flow regime was in its interflow phase.

A plot of the baseflow along the transect is shown in Figure 4 which indicates that a significant increase in flow (groundwater discharge) occurs at high altitude above Linzor, amounting to 0.43 m³/s in October 1999.

Not included in the transect but measured in October 1999, outflow from El Tatio to the south was measured at 0.19 m³/s and to the north, discharge was measured at 0.195 m³/s in the upper Loa (localities 12+13). Thus the combined baseflow from intra-arc aquifers to the Río Loa catchment based on the instantaneous water balance was 0.815 m³/s at the end of the dry season,



compared with a mean of $0.972 \text{ m}^3/\text{s}$ throughout the year estimated from the recession analysis. These estimates of flow from the intra-arc aquifers reinforce their importance as reservoirs supporting baseflow throughout the Loa catchment.

Downstream from Linzor between 340 and 350 km distance from the ocean, baseflow loses $0.4 \text{ m}^3/\text{s}$ to unnamed formations (potentially an extension to the Jalquinche Formation of the Calama Basin) underlying the Sifon Ignimbrite which is breached by erosion in the Toconce gorge. A small gain of $0.05 \text{ m}^3/\text{s}$ occurs in the vicinity of Toconce (330–340 km from the ocean) due to drainage from the last downstream exposure of the Jalquinche Formation. On the transect, the Calama Basin phreatic aquifers receive leakage of $0.21 \text{ m}^3/\text{s}$ from the Río Salado in the vicinity of Chiu Chiu and again to the Río Loa of $0.43 \text{ m}^3/\text{s}$ at Cascad (locality 7). The last loss ($0.05 \text{ m}^3/\text{s}$) before the ocean occurs in the vicinity of Quillagua to the Quillagua Formation. Finally, below Quillagua there is a small gain ($0.01 \text{ m}^3/\text{s}$) from the Salar de Llamara aquifers (here the Quebrada Amarga Formation). In summary, during the dry season baseflow is largely derived from intra-arc aquifers, with a small contribution from the Pampa Tamarugal in the lowest reach. On the other hand the river recharges aquifers in the Pre-Andean and forearc basins.

The interflow regime in March 2000 shows higher flow rates as expected (Table 2; Figure 4), but the pattern of gains and losses show several important changes. Intra-arc aquifers are still providing significant (inter-) flow ($0.67 \text{ m}^3/\text{s}$), with an additional $0.24 \text{ m}^3/\text{s}$ downstream at 330 km. Leakage ($0.37 \text{ m}^3/\text{s}$) to the presumed Jalquinche Formation occurs between 332 and 342 km and again at 329 km, ($0.29 \text{ m}^3/\text{s}$). However, throughout the Calama Basin from the point where rivers exit the Cordillera to the passage through the Pre-Cordillera, instead of losses there are gains to the river, reaching a maximum of $1.11 \text{ m}^3/\text{s}$ at Cascad, indicating a reversal of flow

when compared with the dry season. In the Central Depression, losses are again observed from the Río Loa to the Quillagua Formation, but with increased rates ($0.35 \text{ m}^3/\text{s}$) compared with the dry season.

4 Hydrogeochemistry

4.1 Sampling and analysis

During October 1999, 22 baseflow samples were taken from surface waters at the gauging sites discussed above, as well as other selected locations. Surface water samples were passed through a $0.45 \mu\text{m}$ filter in the field before being measured for pH, temperature and subsequently sealed in airtight 1 L bottles before transport to the laboratory for analysis. In addition, volume weighted samples of precipitation were collected from six sites during the period December 1999 to March 2000. These samples were collected by the DGA from selected rain gauge stations in the Cordillera. At each station the rain gauges were decanted immediately after storm events into small airtight bottles which were sealed and stored at $\sim 4^\circ\text{C}$ until the end of the wet season when samples were aggregated for each station before being sent to the laboratory for analysis. The snow sample from Cerro Aucanquilcha is a bulk sample collected on 25 March 2000, 300 m above the snowline and 10 days after the storm event of 15 March that produced the snowfall. The snow sample from Cerro Cupo is also a bulk sample taken on 5 June 2000, 200 m above the snowline and 3 days after the storm event of 2 June from which the snow derived. Laboratory analyses were undertaken by ALS in Antofagasta, using ion chromatography for anions (Cl , SO_4 , NO_3), volumetric titration for HCO_3 , atomic absorption spectroscopy for cations (Na , K , Ca , Mg , As) and colorimeter

TABLE 3 Precipitation chemistry.

SampleID	Location†	Sample origin	Date sampled	Precip DJFM 1977-1991	Precip DJFM 2000	2000/1977-1991	Lat	Long	Elevn	pH	TDS calc	Na	K	Ca	Mg	SO ₄	Cl	Na/Cl	K/Cl	Ca/Mg
				mm		%			m a.s.l			mg/L								
W-PPASC/31	Ascotan	cum RF Dec-Mar	20/03/2000	46.2	76	165	-21.73	-68.28	3,956	6.5	62.4	22.9	2.7	9.9	0.8	21	28	0.82	0.10	12.1
W-PPCCH/29	Colchane	cum RF Dec-Mar	20/03/2000	85.8	107	125	-19.73	-68.64	3,717	6.5	25.5	4.2	1.0	2.6	0.8	11	10	0.42	0.10	3.3
W-PPCOL/30	Collacagua	cum RF Dec-Mar	20/03/2000	92.6	137	148	-20.04	-68.83	3,990	6.5	14.5	1.6	1.4	2.7	0.4	5	5	0.32	0.28	7.1
W-PPET/32	El Tatio	cum RF Dec-Mar	20/03/2000	93.4	228	244	-22.37	-68.01	4,345	6.5	11.6	1.8	0.3	1.2	0.1	5	5	0.36	0.06	8.4
S-NVAUC/28	Co Aucanquilcha	snow after 10 days	25/03/2000				-21.23	-68.49	5,175	5.1	2.5	0.17	0.07	0.31	0.07	1	1	0.17	0.07	4.4
S-CUPNV/2	Cerro Cupo	snow after 3 days	05/06/2000				-22.06	-68.31	3,796	4.5	2.9	0.12	0.15	0.7	0.08	1	1	0.12	0.15	8.8
	Western Cordillera rainfall mean (Colchane, Collacagua, El Tatio)*										17.18	2.52	0.91	2.17	0.44	7.00	6.67	0.38	0.14	4.98
	Amazonia rainfall mean**										1.17	0.20	0.05	0.05	0.02	0.52	0.33	0.38	0.13	2.20
	Seawater (mean/1,000)**										34.24	10.56	0.38	0.40	1.27	2.65	18.98	0.56	0.02	0.31

† plotted as nominal 450 km from ocean in [Figures 5, 6 and 9](#).

* this study, excluding snow and Ascotan.

** [Faure \(1997\)](#).

for SiO₂. The results of the analyses are reported in Tables 3 for precipitation, and 4 for surface waters. Ion balance errors for the surface water sampled averaged 4.2% ($\pm 2.3\%$, 1σ). PHREEQC (Parkhurst and Appelo, 2013) was used to calculate P_{CO_2} , and saturation indices (SI) for calcite, dolomite and gypsum (see Supplementary Material S5).

At selected sites, samples were taken for stable isotope, ultra low-level ³H, $\delta^{13}\text{C}_{\text{DIC}}$ and $^{14}\text{C}_{\text{DIC}}$ analysis at the GNS Science Laboratory in New Zealand. Field sampling followed the same protocols as above, whilst samples for AMS $^{14}\text{C}_{\text{DIC}}$ determination were stabilized with HgCl₂. Samples were stored in the dark at $\sim 4^\circ\text{C}$ until transport to the laboratory. Stable isotope measurements are with respect to VSMOW with error limits of $\pm 1.0\text{‰}$ for $\delta^2\text{H}$ and $\pm 0.1\text{‰}$ for $\delta^{18}\text{O}$. Ultra-low level ³H determinations have a detection limit of 0.05 TU. *In-situ* production of ³H by fission of ²³⁸U and/or ⁶Li in magmatic rocks has been calculated at $\ll 0.05$ TU (Goff and McMurtry, 2000), so no allowance for these sources of ³H need be made. $\delta^{13}\text{C}_{\text{DIC}}$ measurements are with respect to VPDB with a precision of 0.2‰. $^{14}\text{C}_{\text{DIC}}$ results are normalized to $\delta^{13}\text{C}_{\text{DIC}}$ at -25‰ . The $^{14}\text{C}_{\text{DIC}}$ detection limit is ± 1 pmC and determinations have a precision of 1%–2%. The results are presented in Table 5.

4.2 Precipitation chemistry

The summer rainfall season of 1999–2000 was significantly wetter than average due to the impact of cold phase ENSO (La Niña) conditions that persisted from the end of 1998 through early 2001. The possibility exists therefore that the sample results are biased toward wetter than average conditions. Nevertheless, since there are few other major ion analyses available for precipitation in the region, they are presented here as an important aspect constraining the hydrogeochemical system.

TDS concentrations vary from 12 to 26 mg/L, excluding Ascotan with a maximum of 62 mg/L. The latter shows high Na, Ca, SO₄ and Cl concentrations indicating contamination from deflated gypsum and halite in the nearby salar. Snow is significantly lower, < 3 mg/L and depleted in all ions as a result of leaching during snowmelt in the time between deposition and sampling (Hornbeck, 1986). Hence snow samples do not reflect the original composition of the precipitation. Although ionic concentrations are around 15–20 times greater than Amazonian precipitation (Faure, 1997), ion ratios indicate a greater affinity with Amazonian precipitation than with seawater. This is consistent with an easterly source expected during La Niña conditions (Cai et al., 2020; González-Pinilla et al., 2021).

4.3 River water chemistry

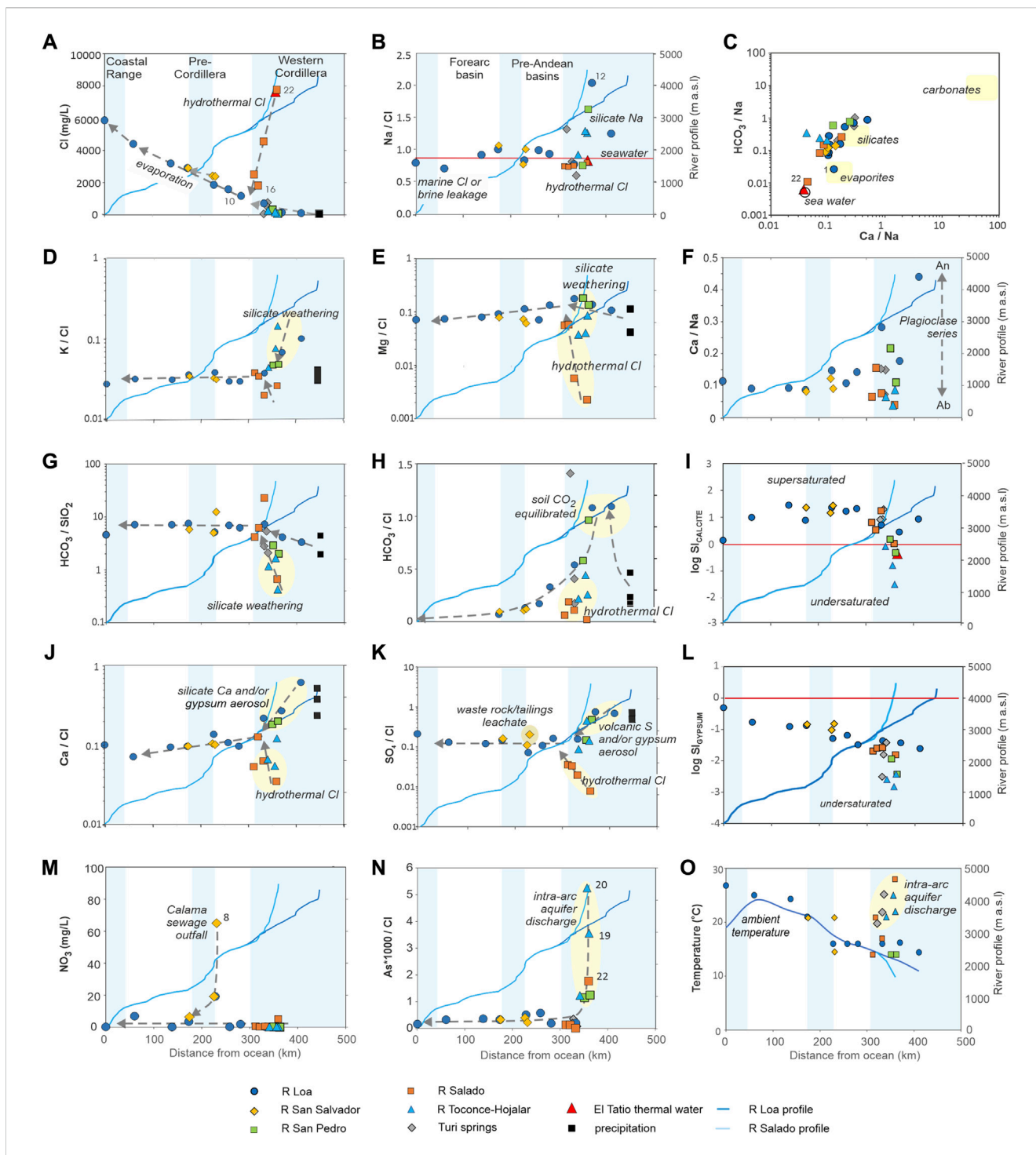
Chloride evolution through the catchment resolves into a dual process when Cl is plotted against distance from the ocean (Figure 5A). The first process is a gradual increase in concentration in the Río Loa and its tributaries, due to either evaporation of baseflow or dissolution of evaporitic minerals along the flow path (or both). The second process in the Río Salado and its tributaries, points to a gradual dilution of Cl from 7,760 mg/L at the exit to the El Tatio hydrothermal system, to

2,510 mg/L at locality 16 just before the confluence with the Río Loa. This process is interpreted to be the result of dilution of Cl-rich thermal water by incremental discharge from moderate to low-Cl intra-arc aquifers. The molar ratio of Na:Cl is close to 1 in the Pre-Andean and Forearc basins, suggesting the dissolution of halite, but subtle differences may be noted elsewhere (Figure 5B). Within the Western Cordillera excess Na (Na:Cl > 1) is likely due to silicate weathering, whereas Na depletion (Na:Cl < 1) is found in the hydrothermal waters. Downstream, below Quillagua, the molar Na:Cl ratio (0.701) is somewhat lower than sea water which may suggest that leakage of salts from the Salar de Llamara brine is more likely than dissolution of deposited marine aerosols (Rech et al., 2003; Wang et al., 2014; Voigt et al., 2020).

The Na normalized plot of HCO₃ to Ca ratio in Figure 5C indicates that the majority of baseflow samples plot close to the silicate weathering field (Gaillardet et al., 1999). There are two outliers: locality 1 next to the ocean plots close to the evaporite field, and locality 22 which is the outlet from the El Tatio hydrothermal field. No samples plot close to the carbonate field, so calcite dissolution appears to be unimportant. High silicate loads associated with rock weathering and geothermal activity are particularly noticeable in the headwaters of the Ríos Loa, San Pedro, Toconce and Hojalar as variously indicated by high Na, K, Ca and Mg to Cl ratios, low HCO₃:SiO₂ ratios and temperatures above ambient (Figures 5B,D,E,G,J,O respectively). Within the Western Cordillera the molar Ca:Na ratio varies widely between 0.04 and 0.49, but after the rivers descend below 3,000 m, the Ca:Na ratio remains stable at around 0.1, suggesting that silicate weathering is limited to higher elevations and volcanic rocks. Based on the Ca:Na ratios within the Cordillera, the principal source rock is rich in plagioclase (An₃₀₋₉₀) and associated ferromagnesian minerals (high K and Mg) consistent with the petrology of the widespread Miocene-Pleistocene lavas and pyroclastic rocks that range from andesites to dacites with a high percentage of unstable glass and some olivine (de Silva, 1989; Godoy et al., 2014; Godoy et al., 2017; González-Maurel et al., 2020).

The corresponding carbonate system is illustrated in Figures 5H,I pH increases from slightly acidic rain (pH = 6.5, Table 3) to slightly alkaline (8.0 ± 0.4 , 1σ) throughout the flow regime, so that dissolved inorganic carbon (DIC) is virtually all HCO₃ (Table 4). The zone between 3,500 and 4,500 m has an extensive cover of cushion plants and tussock grasses that respire CO₂ (Houston, 2009), causing soil water to be enriched in HCO₃. As the rivers descend from this elevation, they lose HCO₃, which coupled with Ca released from silicate weathering and/or deflated gypsum incorporated from nearby salars in the presence of P_{CO_2} well above atmospheric in all samples, quickly proceeds towards calcite saturation (Figure 5I, Supplementary Material S5). Downstream throughout the Calama and Turi Basins the rivers maintain calcite saturation with travertine and calcareous tufa being deposited along their course as degassing of CO₂ takes place. Dolomite saturation follows a similar path to calcite and is supersaturated in rivers after they leave the Cordillera.

The headwaters of the Ríos Loa, San Pedro and Toconce present molar SO₄:Cl of ~ 1 (Figure 5K) decreasing downstream to ~ 0.1 , suggesting high elevation volcanic S sources, and/or gypsum aerosol deposition from nearby salars, notably Ascotan. Conversely, the Río Salado headwaters have comparatively low SO₄ given that phase



separation at depth within the El Tatio hydrothermal system allows for the production of peripheral acid-sulphate springs (Giggenbach, 1978). However, the same author reports flow rates amounting to $0.012 \text{ m}^3/\text{s}$ (95% total) for the mature Cl springs and only $0.0006 \text{ m}^3/\text{s}$ (5% total) for the SO_4 springs, which would explain the low SO_4 concentration in the Río Salado. Downstream from El Tatio, dilution

of Cl increases the $\text{SO}_4:\text{Cl}$ molar ratio. Once the rivers leave the Cordillera, the $\text{SO}_4:\text{Cl}$ ratio maintains a constant 0.1 as far as Quillagua. Thereafter a rise in sulphate from 770 mg/L to 1750 mg/L is mirrored by increases in Ca, Na and Cl, coupled with a decrease in HCO_3^- . This change may be associated with the dissolution of marine aerosol deposition (Rech et al., 2003) or groundwater inflow (halite and

TABLE 4 Surface water chemistry compared with groundwater chemistry (sources indicated).

Fig 1&8 ref #	Location	River system	Date	Lat	Long	Altitude	Dist from ocean	pH	Temp	TDS calc	Na	K	Ca	Mg	HCO ₃	SO ₄	NO ₃	Cl	SiO ₂	As	ion balance
						m a.s.l	km		°C		mg/L										%
THIS STUDY: baseflow																					
1	Rio Loa al mar	Loa	10/99	-21.43	-70.04	25	0	7.0	26.8	11,940	3,000	175	659	287	209	1750	0.2	5,860	45	2.0	4.3
2	Rio Loa Quillagua	Loa	10/99	-21.67	-69.54	750	60	7.8	25.0	8,273	2000	152	350	224	377	770	6.9	4,400	52	3.0	7.9
3	Cruce Las Torres	Loa	10/99	-22.28	-69.97	1,150	138	8.7	25.0	6,648	1890	108	337	174	433	516	0.1	3,190	60	2.4	4.5
4	Rio Loa Chacance	Loa	10/99	-22.40	-69.52	1,185	173	7.8	21.0	6,427	1885	114	314	183	441	580	3.5	2,910	58	2.0	6.7
5	Rio San Salvador Chacance	San Salvador	10/99	-22.40	-69.53	1,190	175	8.1	20.8	6,599	2000	109	315	157	478	630	6.4	2,910	81	2.0	6.2
6	Ojos de Opache	San Salvador (sp)	10/99	-22.48	-69.00	2065	226	7.9	20.8	4,912	1,200	86	283	121	442	360	19.2	2,420	87	2.0	3.9
7	Rio Loa Cascad	Loa	10/99	-22.51	-68.98	2,180	228	8.1	16.0	3,986	1,000	99	284	145	418	180	0.6	1,860	80	2.0	5.7
8	Rio San Salvador above Opache	San Salvador	10/99	-22.45	-68.97	2,100	231	8.2	14.5	5,519	1,545	81	270	100	492	651	65.0	2,380	39	1.1	0.1
9	Rio Loa Angostura	Loa	10/99	-22.46	-68.73	2,460	258	8.0	16.0	4,233	1,210	61	227	92	478	275	2.2	1,890	68	2.0	6.4
10	Rio Loa Lasana	Loa	10/99	-22.27	-68.63	2,580	281	8.4	16.0	2,401	578	31	104	88	430	210	1.9	960	68	0.3	6.0
11	Rio Loa above Conchi	Loa	10/99	-21.95	-68.61	3,010	333	8.0	16.0	2,159	353	29	173	86	658	150	<0.2	710	90	0.3	3.2
12	Rio Loa above Lequena	Loa	10/99	-21.68	-68.66	3,314	370	7.8	16.2	920	190	16	65	20	268	217	<0.2	144	94	0.2	1.1
13	Chela	Loa (sp)	10/99	-21.35	-68.60	3,766	411	8.3	14.4	598	88	12	75	8	205	101	<0.2	109	97	0.2	2.3
14	Ojos de San Pedro	San Pedro	10/99	-21.98	-68.36	3,780	351	8.3	16.0	1,010	160	17	67	41	329	66	<0.2	330	112	0.8	7.7
15	Incaliri	San Pedro (sp)	10/99	-22.03	-68.07	4,050	363	8.0	14.0	359	80	4	17	7	126	49	<0.2	76	62	0.2	3.0
16	Rio Salado Chiu Chiu rd	Salado	10/99	-22.33	-68.56	2,555	312	8.0	14.0	4,444	1,200	104	150	97	263	120	0.6	2,510	62	0.7	5.5
17	Rio Salado Sifon	Salado	10/99	-22.29	-68.34	2,890	321	8.0	20.0	3,751	860	68	258	72	591	82	<0.2	1,820	94	0.5	5.1
18	Rio Toconce at Toconce repr	Toconce	10/99	-22.27	-68.15	3,300	341	8.1	21.0	605	160	13	20	7	102	33	<0.2	270	86	0.7	6.5

(Continued on following page)

TABLE 4 (Continued) Surface water chemistry compared with groundwater chemistry (sources indicated).

Fig 1&8 ref #	Location	River system	Date	Lat	Long	Altitude	Dist from ocean	pH	Temp	TDS calc	Na	K	Ca	Mg	HCO ₃	SO ₄	NO ₃	Cl	SiO ₂	As	ion balance
						m a.s.l	km		°C		mg/L										%
19	Rio Toconce at Linzor	Toconce/Hojalar (sp)	10/99	-22.23	-68.03	4,050	360	7.3	22.0	293	70	14	12	5	38	69	<0.2	86	88	0.6	1.8
20	Rio Hojalar above Linzor	Toconce/Hojalar	10/99	-22.34	-67.98	4,480	356	8.1	25.0	531	150	15	11	5	137	33	<0.2	180	81	2.0	1.3
21	Rio Salado	Salado	10/99	-22.28	-68.23	3,060	332	7.7	17.0	8,323	2,200	99	321	178	855	120	0.5	4,550	37	0.1	6.5
22	El Tatio outflow	Salado	10/99	-22.33	-68.03	4,228	359	7.4	28.0	12,492	4,000	221	303	12	114	82	5.1	7,760	169	29.0	6.8
T1	Cupo	Turi (sp)	10/99	-22.11	-68.31	3,370	338	8.1	25.0	2,167	336	38	170	111	532	160	0.2	820	111	0.05	6.8
T2	Paniri	Turi (sp)	10/99	-22.14	-68.27	3,260	330	8.3	19.0	563	100	2	53	13	269	16	0.2	110	92	0.05	4.2
T3	Banos de Turi	Turi (sp)	10/99	-22.23	-68.28	3,050	335	6.2	22.0	1920	419	45	120	45	437	114	0.2	740	46	0.20	0.1
THIS STUDY: interflow																					
1	Rio Loa al mar	Loa	03/00	-21.43	-70.04	25	0	5.7	26.8	10,656	2,980	145	555	264	132	1,220	n/a	5,360	59	3.2	0.3
2	Rio Loa Quillagua	Loa	03/00	-21.67	-69.54	750	60	7.6	24.5	7,999	2,270	124	420	217	276	632	n/a	4,060	63	3.6	2.4
4	Rio Loa Chacance	Loa	03/00	-22.40	-69.52	1,185	173	8.8	20.8	6,487	1,850	100	312	169	202	454	n/a	3,400	62	2.3	1.0
5	Rio San Salvador Chacance	San Salvador	03/00	-22.40	-69.53	1,190	175	8.6	14.5	5,564	1,500	100	320	150	233	481	n/a	2,780	75	1.8	1.2
6	Ojos de Opache	San Salvador (sp)	03/00	-22.48	-69.00	2,065	226	7.6	16.0	4,552	1,160	75	283	120	202	332	n/a	2,380	74	1.9	1.6
7	Rio Loa Cascad	Loa	03/00	-22.51	-68.98	2,180	228	8.1	16.0	5,190	1,490	78	273	129	242	298	n/a	2,680	72	1.7	2.2
9	Rio Loa Angostura	Loa	03/00	-22.46	-68.73	2,460	258	7.7	14.5	3,431	920	55	180	83	233	161	n/a	1,800	57	1.1	1.4
10	Rio Loa Lasana	Loa	03/00	-22.27	-68.63	2,580	281	7.3	16.0	1,503	320	29	95	75	221	189	n/a	574	62	0.2	2.8
11	Rio Loa above Conchi	Loa	03/00	-21.95	-68.61	3,010	333	7.6	16.3	1,846	391	28	159	77	314	200	n/a	678	74	0.2	4.6
14	Ojos de San Pedro	San Pedro	03/00	-21.98	-68.36	3,780	351	7.7	14.0	666	134	17	44	36	151	85	n/a	199	69	0.5	6.4
16	Rio Salado Chiu Chiu rd	Salado	03/00	-22.33	-68.56	2,555	312	7.2	14.5	3,350	996	73	136	66	239	99	n/a	1,740	63	1.2	1.5

(Continued on following page)

TABLE 4 (Continued) Surface water chemistry compared with groundwater chemistry (sources indicated).

Fig 1&8 ref #	Location	River system	Date	Lat	Long	Altitude	Dist from ocean	pH	Temp	TDS calc	Na	K	Ca	Mg	HCO ₃	SO ₄	NO ₃	Cl	SiO ₂	As	ion balance
						m a.s.l	km		°C	mg/L											%
17	Rio Salado Sifon	Salado	03/00	-22.29	-68.34	2,890	321	7.8	16.2	2,671	800	53	166	46	235	101	n/a	1,270	103	1.3	6.3
18	Rio Toconce at Toconce repr	Toconce	03/00	-22.27	-68.15	3,300	341	6.6	20.8	328	80	14	15	6	48	65	n/a	100	79	0.7	0.4
19	Rio Toconce at Linzor	Toconce/Hojalar (sp)	03/00	-22.23	-68.03	4,050	360	7.3	22.0	314	85.4	13	12	5	37	73	n/a	88	75	0.7	4.0
20	Rio Hojalar above Linzor	Toconce/Hojalar	03/00	-22.34	-67.98	4,480	356	8.8	21.0	273	64.5	17	8	5	68	19	n/a	92	75	0.9	1.4
21	Rio Salado	Salado	03/00	-22.28	-68.23	3,060	332	7.6	16.3	6,839	2,100	76	409	158	283	93	n/a	3,720	53	0.0	5.6
22	El Tatio outflow	Salado	03/00	-22.33	-68.03	4,228	359	7.9	32.0	4,613	1,630	123	87	10	77	75	n/a	2,610	106	15.5	1.5
T1	Cupo	Turi (sp)	03/00	-22.11	-68.31	3,370	338	8.1	15.0	2,400	349	40.9	165	126	299	208	n/a	861	105	0.80	0.7
T3	Banos de Turi	Turi (sp)	03/00	-22.23	-68.28	3,050	335	6.41	17.5	3,040	381	49.3	97.2	44.2	205	96	0.19	720	96	0.48	0.3
Groundwater studies																					
TURI	this study	single sample		upper aquifer		330*	7.7	19	2,806	330	32	104	63	299	102	<0.2	809	80	0.3		
		single sample		lower aquifer		330*	5.2	21	9,608	3,610	162	57.1	90.7	99	189	<0.2	5,400	2	2.9		
	Godfrey et al., 2019	mean of 3 samples		springs		335*	7.5	2,207	191	386	144	79	426	206	n/a	777					
CALAMA NORTHERN AQUIFERS	Herrera et al., 2021	mean of 8 samples		upper aquifer		265*	7.4	21	2,751	680	44	122	62	365	280	<0.2	1,199				
		mean of 11 samples		lower aquifer		265*	7.4	8	2,492	695	42	196	74	391	410	<0.2	1,313				
CALAMA SOUTHERN AQUIFERS	this study	mean of 8 samples		upper aquifer		280*	7.0	25	3,045	1,017	59	322	108	270	155	0.2	2003	71	1.2		
		mean of 4 samples		lower aquifer		45*	6.4	33	11,756	3,218	156	1,023	142	633	490	1.2	6,095	38	0.0		
SALAR DE LLAMARA	Lopez et al., 1999 Otalora et al., 2020	minimum value† of 109 samples		surface pits		45*	n/a	n/a	23,405	7,478	222	331	141	111	5,830	n/a	9,291				

* plotting position for Figure 9 nominal.

† considered representative of near-surface groundwater throughflow.

Sp - surface water source spring.

TABLE 5 Surface water and precipitation isotope analyses.

Figs 1 & 8 ref #	Location	River system	Date	Lat	Long	Altitude	Dist from ocean	$\delta^{18}\text{O}$	$\delta^2\text{H}$	d	^3H		DIC	log P_{CO_2}	$\delta^{13}\text{C}_{\text{DIC}}$	$^{14}\text{C}_{\text{DIC}}$	
								VSMOW	VSMOW		‰	‰			‰	TU	+/-
						m a.s.l	km	‰	‰	‰			mmol/L		‰	pmC	+/-
1	Rio Loa al mar	Lower Rio Loa	10/99	-21.43	-70.04	25	0	-4.17	-52.37	-19.0			3.9	-1.83	-5.39	113.48	0.74
4	Rio Loa Chacance	Lower Rio Loa	10/99	-22.40	-69.52	1,190	173	-5.66	-60.99	-15.7	1.25	0.2	7.8	-2.56	-9.93	107.29	0.81
11	Rio Loa above Conchi	Upper Rio Loa	10/99	-21.95	-68.61	3,010	333	-8.46	-74.45	-6.8	0.5	0.1	11.7	-1.55	0.63	6.93	0.16
14	Ojos de San Pedro	San Pedro	10/99	-21.98	-68.36	3,780	351	-9.69	-81.35	-3.8	0.3	0.3	5.8	-1.92	1.67	4.82	0.14
15	Inacaliri	San Pedro	10/99	-22.03	-68.07	4,050	363	-12.41	-91.58	7.7			2.1	-2.71	-5.55	31.25	0.37
17	Rio Salado Sifon	Rio Salado	10/99	-22.29	-68.20	2,890	321	-6.90	-54.06	1.1	0.9	0.2	11.0	-1.41	2.13	11.02	0.21
20	Rio Hojalar above Linzor	Toconce	10/99	-22.34	-67.98	4,480	356	-7.90	-62.59	0.6	0.8	0.2	1.6	-3.12	-18.53	13.07	0.42
21	Rio Salado	Rio Salado	10/99	-22.28	-68.23	3,060	332	-7.72	-64.84	-3.1			6.8	-2.73	5.44	6.52	0.14
22	El Tatio outflow	Rio Salado	10/99	-22.33	-68.03	4,228	359	-6.50	-54.60	-2.6			2.0	-2.48	-20.10	50.70	0.61
T1	Cupo	Turi sp	10/99	-22.16	-68.33	3,175	342	-7.72	-57.26	4.5	0.6	0.2	8.6	-2.47	5.64	6.73	0.14
T2	Paniri	Turi sp	10/99	-22.15	-68.27	3,281	339	-7.47	-46.28	13.48	0.8	0.2	4.3	-2.91	-1.20	4.65	0.17
T3	Baños de Turi	Turi sp	10/99	-22.23	-68.28	3,091	331	-7.76	-53.1	8.98	0.96	0.2	5.8	-1.17	4.65	2.17	0.20
	Pptn Ascotan	rain*	Dec-March 00	-21.73	-68.28	3,956	450*	-11.13	-81.62	7.4	4.73	0.83					
	Pptn Colchane	rain*	Dec-March 00	-19.73	-68.64	3,717	450*	-9.83	-68.33	10.3							
	Pptn Collacagua	rain*	Dec-March 00	-20.04	-68.83	3,990	450*	-11.19	-75.80	13.7							
	Pptn El Tatio	rain*	Dec-March 00	-22.37	-68.01	4,345	450*	-8.90	-59.95	11.3	2.60	0.30					
	Cerro Cupo	snow*	03/00	-21.23	-68.49	5,175	450*	-10.69	-68.42	17.1							
	Co Aucanquilcha	snow*	06/00	-22.06	-68.31	3,796	450*	-14.40	-100.27	14.9							

* plotted as nominal 450 km from ocean in Figure 7

gypsum derived brines) from the Salar de Llamara via the Quebrada Amarga (Rojas et al., 2010; Viguier et al., 2019). In the vicinity of Calama (locality 8) low-volume, high SO₄ and SiO₂ loads discharge to the San Salvador. The source of this input is likely associated with leachate from mining waste rock and tailings dams, some 3 km to the northeast of the Río San Salvador source.

The constant Na, K and SO₄ to Cl ratios downstream throughout the Pre-Andean and forearc basins, coupled with the increase in gypsum saturation (Figures 5B,D,K,L respectively) may be attributed to evaporative concentration, and argues against significant halite dissolution. Gypsum saturation is never sufficient for precipitation from surface waters anywhere in the catchment, unlike calcite and dolomite that are saturated throughout the Pre-Andean and forearc basins. Both Ca and Mg show depletions relative to Cl and Na through these basins, suggesting that they are being removed by calcite precipitation or that cation exchange is taking place. Since Mg:Ca ratios are everywhere below 1, calcite would be the mineral precipitating under current conditions (Tucker and Wright, 1990; Alonso-Zara and Tanner, 2010; deWet et al., 2015).

Nitrate is generally not a significant component of the flow system (Figure 5M), being everywhere less than 0.4 mg/L, except in the Río San Salvador where it reaches a maximum concentration of 65 mg/L close to the outskirts of Calama (locality 8). Its source is observed to be the sewage outlet from the town. Leakage from the Calama sewage collection system permeates the phreatic aquifers in the Opache Formation underlying the town; 19 mg/L at Ojos de Opache (locality 6), and 0.6 mg/L at Cascad (locality 7). At Chacance (locality 5) the Río San Salvador has a NO₃ load reduced to 6 mg/L, whilst the Río Loa (locality 4) has increased to 3.5 mg/L. Such convergence in concentration between the rivers implies mixing occurring in the passage through the Pre-Cordillera incised valley, potentially through the Batea or Calama Formations where they are exposed in the river beds that are ~5 km apart above Chacance.

Arsenic is found throughout the surface water system varying from 0.1 to 29 mg/L, with the highest concentration from the outflow of El Tatio where Munoz-Sáez et al. (2018) report up to 47 mg/L for the upper geyser field. Low levels of SO₄ argue against sulphides as a source for the As. Alternative sources include leaching from ignimbrites (the Sifon contains 16 ppm - Álvarez-Amado et al., 2022, and the Puripicar 23–36 ppm - Youngman, 1984), as well as silicates and carbonates in the crust and mantle. Indeed, Tapia et al., 2020 suggest that As concentrations are positively correlated with crustal thickness, some 75 km under the Western Cordillera at this latitude (Sodoudi et al., 2011). Plots of As:Cl ratios against thalweg distance (Figure 5N) show that the impact of As from El Tatio reduces downstream in the Río Salado as dilution occurs, and subsequent mixing with the Río Loa. Of interest are the high As:Cl ratios found in the Toconce-Hojalar and San Pedro catchments which, together with elevated temperatures, are considered to be indicative of more extensive geothermal activity.

Silica concentrations are generally above 80 mg/L throughout the catchment, reaching more than 80 mg/L and up to 169 mg/L, in subcatchments above 3,000 m where water temperatures are above ambient, suggesting the widespread influence of geothermal activity. With the rather low Ca:Na ratios, alteration of albite-rich feldspar and

ferromagnesian minerals to clay minerals, especially smectite is indicated.

Samples taken in March 2000 are representative of interflow (Table 4). Interflow demonstrates similar processes and fluxes to baseflow samples taken in the previous October, the main difference being a uniform dilution of ionic concentration of 16%–24% (see Supplementary Material S6). This compares with ~36% measured flow excess during interflow which may suggest that interflow chemistry includes a small admixture of water from groundwater storage, although the significantly lower HCO₃ suggests a shorter residence time for precipitation in contact with soil CO₂ in high elevation soils.

4.4 Isotopes

Stable isotope analyses are reported in Table 5. Summer precipitation in 1999/2000 gave δ¹⁸O values between –9 and –14‰, with δ²H varying between –60 and –100‰. A plot of δ²H vs. δ¹⁸O (Figure 6) shows that the local meteoric water line (LMWL) is given by:

$$\delta^2\text{H} = 7.1 \delta^{18}\text{O} + 4.7 \quad (6)$$

which, considering the limited dataset, is indistinguishable from the summer LMWL of Valdivielso et al. (2020). The δ¹⁸O lapse rate for precipitation is –1.3‰/km, somewhat lower than that found by Aravena et al. (1999) and Bershaw et al. (2016), but closer to that found by Villablanca (2009), and Valdivielso et al. (2022) for summer precipitation (–1.5 to –2.8‰/km), supporting the concept that mesoscale convection differences due to topography create variations in precipitation δ (Gat, 2010; Fiorella et al., 2015; Scheihing et al., 2017; Valdivielso et al., 2022).

Surface waters diverge from the LMWL along paths indicative of evaporitic enrichment with a slope (Δs) equal to 4.8. The evaporation lines (EL) have dissimilar departures from the LMWL at –14‰ δ¹⁸O for the Río Loa and –11‰ for the Río Salado. Based on the lapse rate, Río Loa waters originate from precipitation at around 6,000 m, whereas Río Salado waters originate from ~4,000 m. This is broadly consistent with the local watershed elevation and the cloud base in the respective source areas. Turi Basin spring waters straddle the LMWL (Figure 6A) and the Salado EL showing a significant meteoric component in these spring waters.

Progressive downstream enrichment of δ¹⁸O indicates evaporitic fractionation during overland and in-channel flow. Based on a simplified Rayleigh equation:

$$\delta^{18}\text{O}_{\text{final}} - \delta^{18}\text{O}_{\text{initial}} = (\epsilon^{18}\text{O}_{w-v} + \Delta\epsilon\text{O}_{w-v}) * \ln f \quad (7)$$

where ΔεO_{w-v} is the kinetic enrichment factor between water and vapor, *f* is the residual water fraction (Clark, 2015), and with enrichment assumed complete at –55 δ²H, the evaporative loss for the Río Loa approximates to 26%, and 16% for the Río Salado (see Supplementary Material S3). For comparison, Figure 6B shows data from Giggenschbach (1978) and Cortecci et al. (2005) for the El Tatio hydrothermal field. Acid sulphate springs show the effect of mixing volatiles from a deep sources with meteoric water, whilst the Cl waters indicate variably sourced meteoric waters mixing with hot fluids from an andesitic reservoir, and stored in aquifers at varying depths (Giggenschbach, 1978; Cortecci et al., 2005; Munoz-Saez et al., 2018).

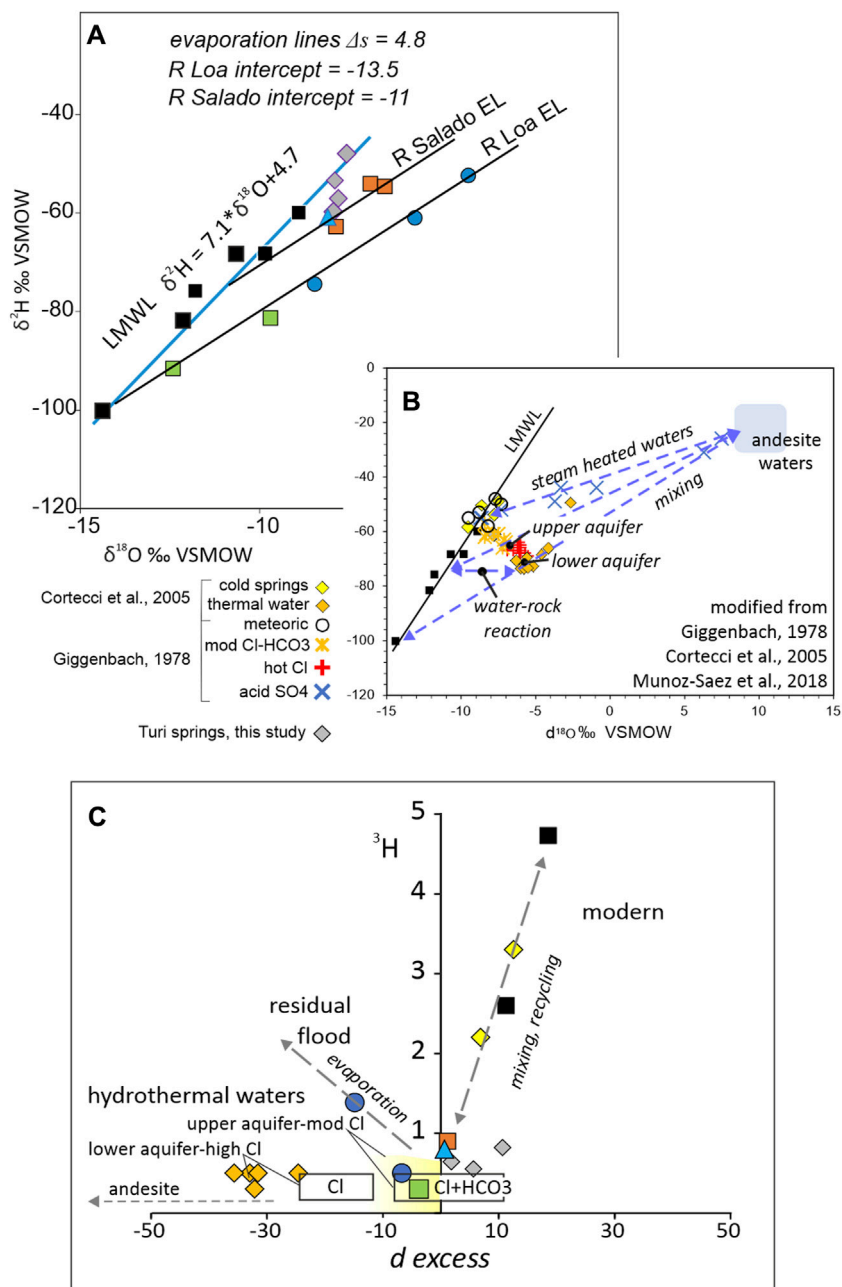


FIGURE 6 Stable isotopes. (A) $\delta^2\text{H}$ vs. $\delta^{18}\text{O}$ showing LMWL and LELs for the Ríos Loa and Salado. (B) stable isotope relations at El Tatio hydrothermal field and their relation to parental andesitic waters based on data sources listed. (C) ^3H to d -excess crossplot with additional data from Cortecchi et al. (2005) and projected data boxes from Giggenbach (1978) for an assumed ^3H value.

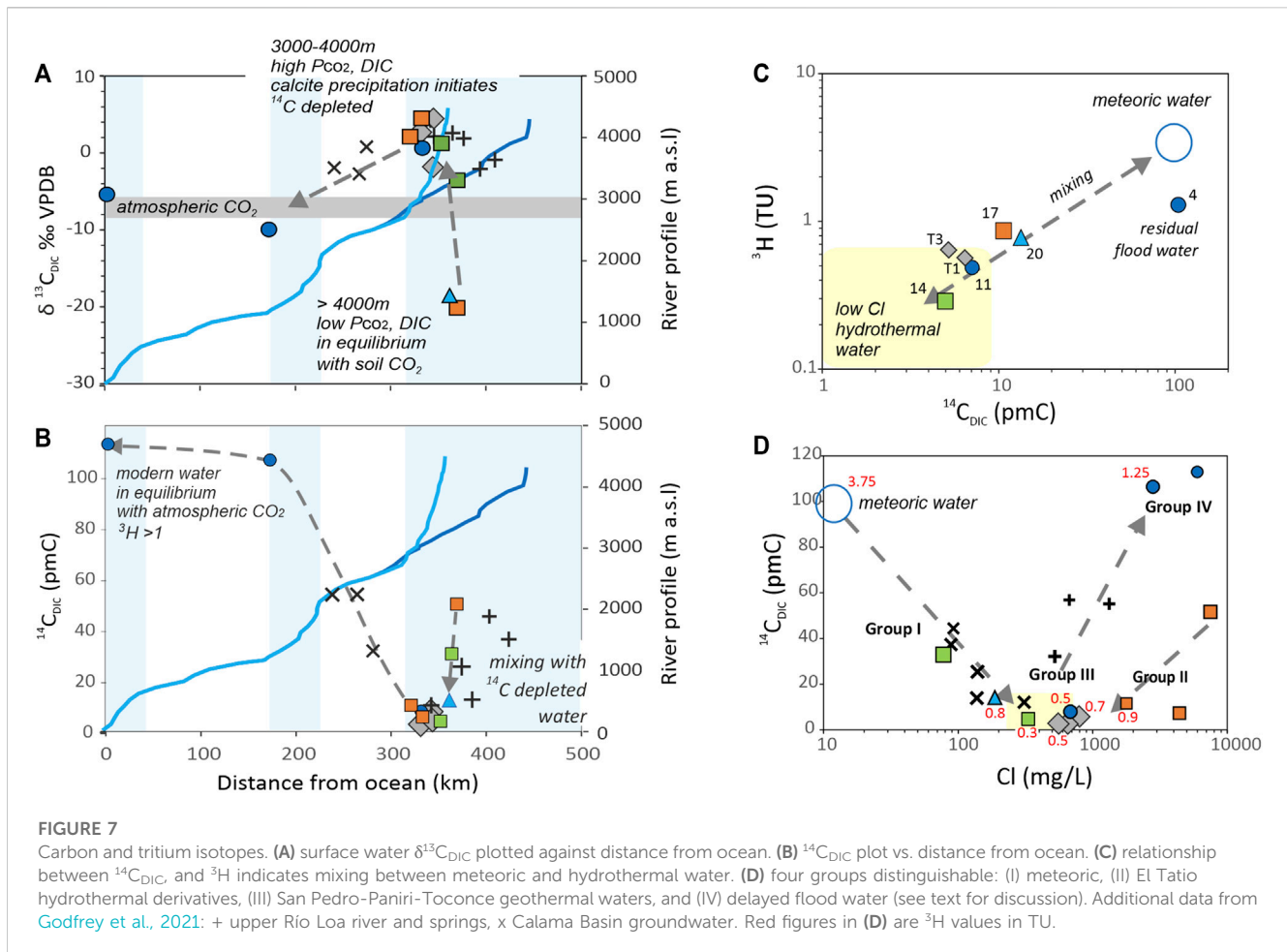
Deuterium excess (d) is a function of source area humidity and is useful in differentiating source area and processes. It is expressed as:

$$d = \delta^2\text{H} - 8\delta^{18}\text{O} \tag{8}$$

In Figure 6C the plot of d against ^3H (as an indicator of water age) reveals hydrothermal waters as old or ^3H depleted. Modern water $^3\text{H} > 2$ TU and d is greater than +10‰, whereas andesite waters are expected to have d around -100‰ with depleted ^3H . From a highly negative d , increasing values are assumed to be the result of incremental volumetric mixing with meteoric waters: hot Cl

waters evolve into moderate Cl+HCO₃ waters, with the HCO₃ component either the result of CO₂ degassing from the hydrothermal plumbing system and/or soil CO₂ generation in recharge waters of near surface reservoirs. There is considerable overlap in the ^3H depleted 0 d region indicating widespread mixing of hydrothermal and meteoric water beyond the limits of the El Tatio geyser field, especially in the Turi samples.

DIC appears to be bimodal in the Cordillera with samples from both the Loa and Salado subcatchments below 7 mmol/L or above 10 mmol/L (Table 5). Below 3,000 m river DIC declines from 8 to 4 mmol/L.



$\delta^{13}\text{C}_{\text{DIC}}$ results are comparably bimodal in the Cordillera (Figure 7A); values between -6‰ and $+6\text{‰}$ could indicate a buried carbonate source but the preferred interpretation here is that these values suggest volcanic CO_2 . In either case, degassing and the initiation of calcite precipitation in both the Ríos Loa and Salado occurs around 3,000 m. $\delta^{13}\text{C}_{\text{DIC}}$ values close to -20‰ are associated with high altitude ($>4,000$ m) sources in equilibrium with soil CO_2 . Farther downstream, in the forearc, $\delta^{13}\text{C}_{\text{DIC}}$ values approximate to atmospheric CO_2 equilibrium at 8‰ reinforcing their identification as residual flood flow.

The presence of ^{14}C in waters may originate from plant respiration, buried carbonates or volcanic volatiles, evolving via mixing and decay during transit. Given this complexity, no attempt is made to apply any age dating model with this data, although $^{14}\text{C}_{\text{DIC}}$ is still invaluable as a tracer. From values around 50 pmC, $^{14}\text{C}_{\text{DIC}}$ decreases downstream in the Western Cordillera (Figure 7B) to <10 pmC, but increases again throughout the Pre-Andean basins to ~ 60 pmC, probably due to the decreased influence of dead volcanic carbon in these aquifers (Godfrey et al., 2021). Values above 100 pmC in the forearc confirm their interpretation as delayed flood waters.

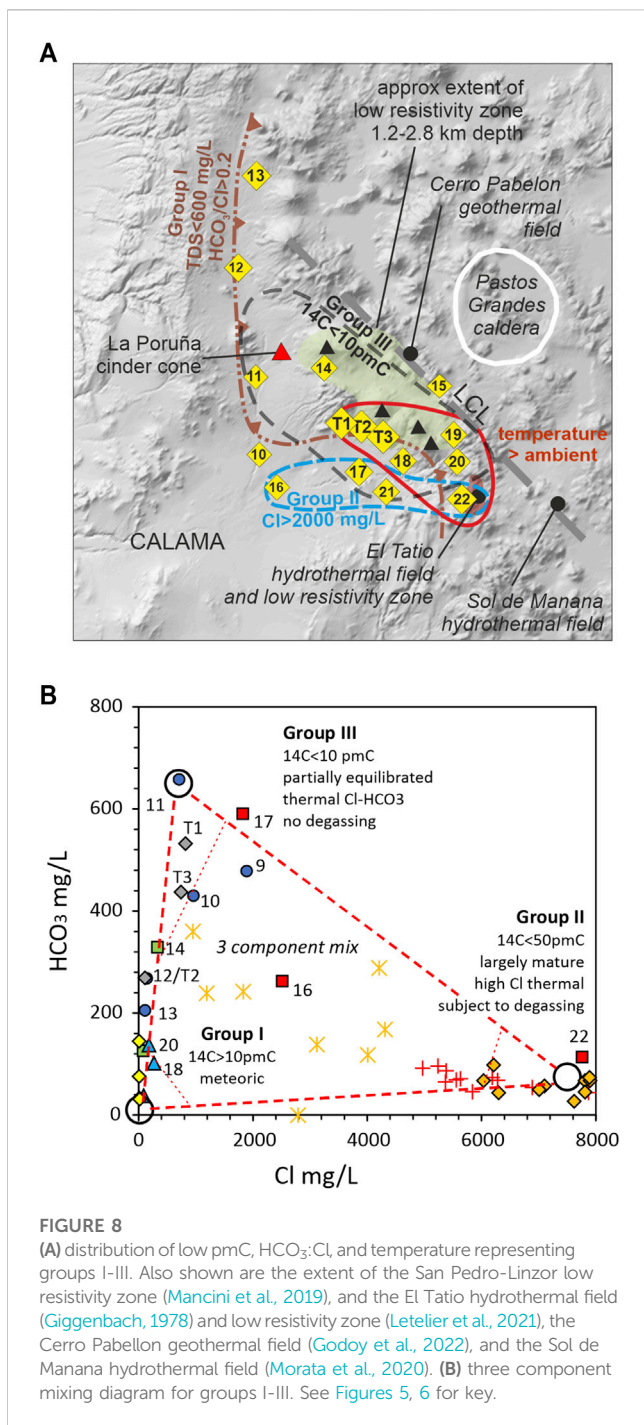
Tritium values in precipitation vary between 2.6 and 4.7 TU, representing modern background levels in the central Andes (Houston, 2006; Moran et al., 2019; Basaldúa et al., 2022). The downstream changes in ^3H mirror those of $^{14}\text{C}_{\text{DIC}}$: at higher elevations in the Cordillera, ^3H decreases towards the Calama Basin (<1 TU) and then increase again in the forearc to >1 TU (Table 5).

The presence of low levels of $^{14}\text{C}_{\text{DIC}}$ are incompatible with measurable ^3H in the same sample (Figure 7C), so that mixing between waters must be invoked. This is complicated by the decreasing then increasing values of $^{14}\text{C}_{\text{DIC}}$ and ^3H as baseflow moves downstream, with the inflexion point at approximately 3,000 m (Figures 7A,B).

4.5 Discrimination of water groups

Four water groups may be recognized based on location, chemistry and isotopic signatures (Figure 7D; Figure 8). Group I waters are found in the San Pedro, Hojalar and Toconce (and probably upper Loa) subcatchments associated with near surface aquifers above 4,000 m. The waters of group I (localities 18, 19, 20) are characterized by relatively dilute TDS (<600 mg/L), molar $\text{HCO}_3:\text{Cl} \sim 0.5$, and d -excess between -10 and $+10\text{‰}$, with ^3H 0.5 to one TU, confirming they are predominately meteoric waters.

Group II waters are exclusively from the Salado subcatchment, originating in the El Tatio hydrothermal system where $\text{HCO}_3:\text{Cl} \sim 0.01$, $\text{SiO}_2 > 100$ mg/L, $^3\text{H} < 1$ TU and d -excess $< 0\text{‰}$ (locality 22). Río Salado samples show decreasing values of $^{14}\text{C}_{\text{DIC}}$ from 50 to 10 pmC downstream, whilst also decreasing in Cl from 7,760 to 1820 mg/L along the flow path. Moderate pmC, together with high Cl and SiO_2 at locality 22 is interpreted as a mix of carbon dead



thermal water (high Cl, SiO₂) (similar or close to a parental magmatic water), with meteoric water that has been in contact with CO₂ in the soil zone. Downstream (localities 17, 21), the fall in pmC and both Cl and SiO₂ suggests the dilution of thermal water with old groundwater discharge.

Group III waters (localities 11, 14, T1, T3) have not previously been identified as a discrete source. They are distinct, having the lowest ¹⁴C_{DIC} (<10 pmC) and ³H (<1 TU), coupled with high HCO₃:Cl (~1) and low SiO₂ of ~70–90 mg/L. These waters are concentrated either side of the Pleistocene San Pedro-Paniri-Toconce volcanic axis including the Turi Basin springs, so that it is hypothesized they originate from a discrete but diffuse ascent of

Cl-rich magmatic water from the APMB (Altiplano-Puna Magma Body) with significant dilution from meteoric waters. Furthermore, their high HCO₃ may develop from conductively cooled thermal waters that lack any volatile release (Fournier, 1989). It is noteworthy that group III waters are closely associated with Volcan Paniri, La Poruña cinder cone and the Chao dacite dome, that have the most recent volcanic activity in the area (respectively 150ka, <100ka, and 56-110 ka) (Godoy et al., 2017; Godoy et al., 2018; González-Maurel et al., 2019; Marin et al., 2020).

Group IV waters, found in the lowest reaches of the Río Loa (localities 1, 2) have high TDS (8,000–12,000 mg/L) as a result of evaporative concentration throughout the river's course, as well as possible mixing/dissolution from Salar de Llamara brines and/or saline marine aerosol deposits (Figure 9) (Rech et al., 2003). Their ¹⁴C_{DIC} ≥100 pmC mark them out as flood waters delayed from the previous wet season.

The acid SO₄ springs that occur at El Tatio and might be considered a separate group, but they represent only ~5% of the total outflow from the geyser field (Giggenbach, 1978), so it is not surprising that SO₄ is not a major component of the surface water system. Fournier (1989) suggested they may represent vapour dominated waters with little outflow.

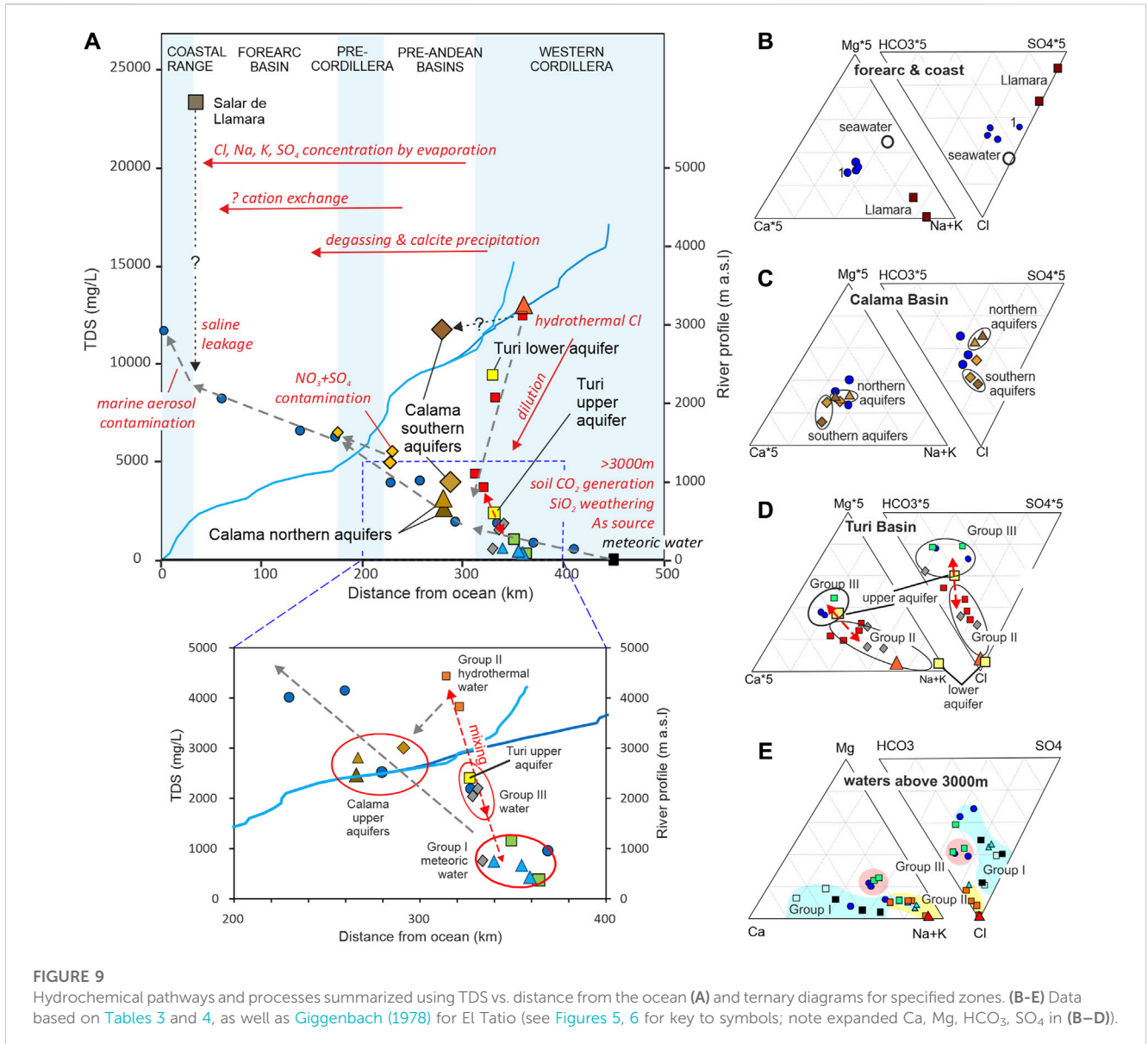
5 Discussion

5.1 Baseflow characteristics and interaction with aquifers

A fundamental control on both streamflow and water chemistry is the annual cycle leading to periods of flood, interflow and baseflow, largely driven by summer (DJF) rainfall. Rising river levels in summer are followed by falling levels during autumn and winter (Mar to Nov). How far floodwater penetrates bank storage, the vadose zone or a contiguous aquifer, causing mixing of waters that have variably evolved, depends on a) the stage head difference between the river and the adjacent vadose zone, b) the duration of positive head difference, c) the degree of hydraulic connection and d) the diffusivity of the adjacent vadose zone or aquifer (Welch et al., 2013).

During flood flow (rising/high stage), there is a tendency for rivers to recharge aquifers throughout their length. During interflow (falling/moderate stage) flow reversal (back-drainage from aquifers) begins in the Cordillera and Pre-Cordillera, whilst the river is still leaking to aquifers in the Central Depression. Finally, during full baseflow (falling/low stage), flow continues to be supplied from intra-arc aquifers, whereas in the Pre-Andean basins and Central Depression river flow reverts to leakage into aquifers, albeit with small fluxes. This cycle of flow into and out of aquifers and/or the vadose zone leads to hysteresis, particularly during falling stages which include mixes from long-lived and evolved aquifer storage, indicating that piston flow may not be a good representation of groundwater transit times (Bethke and Johnson, 2002). As demonstrated by both hydrographs and the instantaneous flow transect, almost 90% of the flow in the Río Loa in the Calama Basin originates from the intra-arc aquifers located above 3,000 m. Throughout the annual cycle, intra-arc aquifers maintain the perennial nature of the flow regime.

Hydrogeochemical processes operating within the catchment may be summarized using TDS vs. location within the catchment,



together with cation-anion ternary plots for each basin (Figure 9). In the intra-arc aquifers above 3,000 m, groups I, II and III dominate, showing the impact of near surface production of carbonic acid in the recharge zone and silicate weathering at depth in the hydrothermal system. Whereas the Río Loa shows increasing TDS downstream due to evaporative concentration or possibly halite dissolution, the Salado catchment is dominated by hydrothermal Cl that is progressively diluted downstream until the two rivers equilibrate solutes near their confluence. Group III waters appear to be a discrete geothermal source of Cl, located along the Paniri-Toconce-Leon volcanic lineament, and mixed with significant HCO₃-rich recharge water. Shallow groundwater in the Turi Basin is shown to be a mix of groups II and III, together with varying mixes of group I, whereas deep groundwater in the Turi Basin is dominated by group II alone.

In the Calama Basin the principal processes operating are degassing and precipitation of calcite, evaporative concentration and localized

contamination of SO₄ and NO₃ in the vicinity of Calama. In the northern sector of the Calama Basin, shallow and deep groundwater as well as shallow groundwater in the southern sector, show strong similarities with surface waters indicating interchange between the river and aquifers. However, the deep southern sector groundwater (which is confined), shows greater affinity with group II than with the rivers. Since the southern lower aquifer groundwater is quite distinct, any hydraulic connection with the upper aquifers or river should be visible as a change in flow rate or chemistry of the latter. However, there are no significant changes either of flow rate or hydrochemistry in the Calama Basin, or in the rivers passage through the Calama gap, so that any outlet from the southern lower aquifer is potentially deep, and/or slow giving time for flows and chemistry to re-equilibrate before discharging.

Passing downstream, evaporative concentration continues across the forearc, and finally, below Quillagua, a sharp increase in TDS may indicate brine leakage from the Salar de Llamara or dissolution of marine aerosol deposits.

Several possibilities exist for the source of water in the intra-arc aquifers: a) direct precipitation infiltration and recharge, b) slab/mantle dehydration, c) deep hydrous crustal melt exsolution and associated metamorphic fluid release, d) near-surface melt decompression and outgassing, e) thermally induced upflow of deeply penetrating meteoric water through buried evaporites or carbonates, and f) far-field recharge. Evaluation of the plausibility of these sources may be approached by considering the variable and invariable components of discharge to rivers from intra-arc aquifers which can be observed in the hydrographs as well as in hydrochemical and isotopic data.

5.2 Variable recharge

The variable component of baseflow changes from year to year and can be correlated with annual rainfall (see [Supplementary Material S2](#)), implying that it represents groundwater discharge following direct precipitation recharge. Variable precipitation recharge (group I water) extends over much of the Western Cordillera in suitable conditions (high-intensity, long-duration precipitation coupled with porous, high-infiltration capacity soils) and its intra-arc aquifers, except where overprinted by group II and III waters. ([Figure 8](#)).

Baseflow recession analysis ([section 3.2](#)) suggests that direct precipitation recharge to intra-arc aquifers above 3,000 m is around 16–23 mm/a ([Table 1](#)). This value compares favorably with two alternative and independent methods of estimating direct recharge. The chloride mass balance technique (CMB), estimates of 1–20 mm/a above 3,000 m but is invalid in areas where volcanic Cl is present ([Houston, 2006c](#)). A soil moisture budgeting algorithm (SMB), estimates 28 mm/a above 4,000 m ([Houston, 2009](#)), and 39 mm/a in the Silala catchment. These recharge amounts give rise to flows of ~0.09 m³/s in the upper Ríos Loa-Salado today, equivalent to only 9% of the total baseflow ([Table 1](#)).

Far-field recharge will be modulated by effective precipitation in its catchment area, thus resulting in variable annual recharge, albeit buffered by distance. Far-field recharge has been suggested to feed the Río Silala above Inacaliri (locality 15) ([Peach and Taylor, 2023](#)). This is supported by the low TDS (<250 mg/L) and high HCO₃:Cl (>1, as mmol/L) ([Aravena et al., 2023](#)). Water balance models ([Muñoz et al., 2023](#); [Peach and Taylor, 2023](#)) have been used to suggest a ~250 km² extension of the groundwater catchment beyond the surface water catchment area. During the period of record (2001–2015) the measured flow in the Río Silala was 0.17 m³/s, never dropping below 0.15 m³/s suggesting the possibility of significant time-invariant flow. Elsewhere, cross-boundary flow has been widely reported ([Anderson et al., 2002](#); [Montgomery et al., 2003](#); [Rissmann et al., 2015](#); [Corenthal, 2016](#); [Boutt et al., 2021](#)). However, neither far-field recharge nor winter precipitation is likely to be able to supply intra-arc aquifer baseflow throughout the year as a result of the overwhelming concentration of precipitation in summer (DJF).

5.3 Invariant recharge

The absence of any significant annual or decadal variation in the time-invariant component of baseflow suggests a long-lived source. Above 3,000 m, two groups of time-invariant recharge water can be distinguished; groups II and III ([Figure 8B](#)).

Group II waters represent a mixture of meteoric and thermal water. The deeply circulating meteoric component supplies modern ¹⁴C with low Cl, whilst the thermal component is ¹⁴C_{DIC} free but Cl rich. The thermal component is assumed to arise from crustal sources ([Aguilera et al., 2012](#); [Mancini et al., 2019](#)) and/or recycled brine at depth ([Risacher et al., 2003](#)).

Group III waters are associated with intra-arc aquifer leakage without significant surface expression. Although these waters appear to be of geothermal origin, as evidenced by ¹⁴C_{DIC} <10 pmC, their lack of surface expression is hypothesized to be the result of argillic capping, hence potentially restricting degassing and leading to retained (high) HCO₃.

5.4 Potential sources of invariant recharge

Despite the identification of two endpoint water types related to the volcanic arc, their sources remain obscure. However, by combining hydrogeological information with geothermal studies it is possible to speculate on the ultimate origin and evolution of these water types. The recycling of water in convergent margins via the descending slab and associated hydrous melts in the crust, leading to the release of aqueous fluid and vapour near surface suggests that these processes may play a role in generating recharge to intra-arc aquifers ([Sparks et al., 2008](#); [Fialko and Pearce, 2012](#); [Ward et al., 2014](#); [Pritchard et al., 2018](#); [Gottsmann et al., 2022](#)). The ascent of H₂O and OH entrained in magma as a fluid, vapour or bound leads to CO₂, Cl, and SO₄ amongst other species, being mobilized ([Zellmer et al., 2015](#)).

[Ingebritsen and Manning \(2002\)](#) calculate that average worldwide subduction dehydration could release between 10⁻⁴–10⁻⁵ m³/s/km² aqueous fluids, which, applied to the area of the upper Ríos Loa and Salado would amount to 0.04–0.27 m³/s, seemingly sufficient to contribute substantially to aquifer recharge. Furthermore, [Schurr et al. \(2003\)](#) and [Wang et al. \(2019\)](#) show that rates vary, with some areas, notably the Western Cordillera having more focused fluxes. A thick crustal passage for volatiles might be indicated by the high As concentrations in the Salado-Toconce-San Pedro subcatchments ([Tapia et al., 2021](#)), as well as He isotope ratios, interpreted by [Hoke et al. \(1994\)](#) and [Barry et al. \(2022\)](#) to indicate ~20% mantle and ~80% crustal volatiles in the discharge from El Tatio and the Western Cordillera. On the other hand, [Risacher et al. \(2011\)](#) argue that the high Cl:Br ratio of thermal waters at El Tatio (average ~2,500 as mmol/L), precluded any subducted seawater component. Yet the same samples have a mean Na:Cl ratio of 0.86, that of seawater.

Low seismic velocities and resistivities at depths of 4–7 and 15–25 km beneath the APVC (Altiplano-Puna Volcanic Complex) have been interpreted as super-hydrous melts (≤10 wt% H₂O) of the APMB ([Chmielowski et al., 1999](#); [Zandt et al., 2003](#); [Ward et al., 2014](#); [Laumonier et al., 2017](#); [Pritchard et al., 2018](#)). [Laumonier et al. \(2017\)](#) estimate the total aqueous mass in the APMB to be 1.4x10¹⁶ kg, which, assuming a fluid density of ±2000 kg/m³ gives a volume of ~7,000 km³. In similar conditions [Hack and Thompson \(2011\)](#) demonstrate that fluid ascent rates between 10⁻⁴–10⁻⁵ m/s depend on the type of flow (porous vs. fissure) and are controlled by pressure, temperature and melt composition. With such reservoir volumes and ascent rates it would easily be feasible to supply continuous recharge to the intra-arc aquifers.

Geochemical models for the hydrothermal system at El Tatio suggest a deep, hot reservoir whose composition is the result of lower crustal magma fractionation leading to andesitic upper crustal fluids and rock-water interactions, coupled with mixing of shallow meteoric waters recharged at higher elevations (Giggenbach, 1978; Cortecchi et al., 2005; Munoz-Saez et al., 2018).

The Paniri-Chao-Leon-Toconce volcanic chain (Figure 1) trends NW-SE displacing the general N-S trend of the volcanic arc. It partially separates the Pre-Andean basins from the intra-arc basins. Forming the Loa-Salado surface watershed to the northeast of the intra-arc aquifers, and parallel to the Paniri-Toconce trend, is the Cordón de Inacaliri-Volcan Linzor trend. These volcanic trends are thought to be controlled by the deep crustal faults associated with the Calama-Olcapato-El Toro and Lipez-Coranzuli lineaments facilitating the ascent of mantle and upper crustal APMB magmas (Godoy and Kojima, 2013; Godoy et al., 2018; Veloso et al., 2020; Hudson et al., 2022). Type III waters are intimately associated with the Paniri-Toconce trend, so it is hypothesized that this pathway, modulated by an extensional crustal regime, has allowed the ascent of aqueous fluids from various levels in the lithosphere.

Low resistivity zones have been located beneath the APVC and notably beneath El Tatio and the San Pedro-Paniri-Toconce trend (Letelier et al., 2021; Montecinos-Cuadros, et al., 2021). These low-resistivity zones occur at depths of <60 m and 200–400 m hinting at possible reservoirs for groups II and III waters. Several hydrothermal, and fumarolic vents associated with argillic alteration are located within and adjacent to the watershed of the Salado (Figure 8) (Scandiffio and Alvarez, 1992; Mancini et al., 2019; Morata et al., 2020; Taussi et al., 2021; Godoy et al., 2022) offering potential pathways for magmatic water to ascend, and mix with surface and groundwater.

The Pastos Grandes Caldera, part of the APMB, and only ~10 km to the NE of the San Pedro Basin is provisionally discounted as an important source for waters in Río Loa catchment as it is associated with carbonate rich fluids that precipitate significant calcareous deposits (Bougeault et al., 2020; Muller et al., 2020), that are not found in the latter under present day conditions. It may however, be the source of small volumes of high-HCO₃, low-Cl waters found in perched and near surface aquifers in the Silala subcatchment (Aravena et al., 2023).

High surficial heat flows (>100 mW/m²—Ibarra and Prezzi, 2019) coupled with a geothermal gradient up to 250 °C/km at Sol de Mañana (Sullcani, 2015) provides a driving mechanism (but not the only) for fluid upflow through the upper crust. Upflow through sediments underlying the APVC potentially alter water chemistry. Risacher and Fritz, (1991), Risacher et al. (2003) and Risacher et al. (2011) consider the Cl content of thermal waters to be buried halite and gypsum, but these are recycled salts, and do not explain the ultimate source of Cl for such evaporites. Here, it is suggested that the ultimate source is found deeper in the crust as a result of magmatic-metamorphic exsolution from the APMB as proposed by Hovland et al. (2018a, 2018b) and found by Rissmann et al. (2015) for the Monturaqui-Negrillar-Tilopozo aquifer that feeds the Salar de Atacama to the south of the Calama Basin.

If voluminous limestones underly the APVC cover, they could represent a deep aquifer and a source for carbonates in groundwater and baseflow. Within the upper reaches of the Salado-Toconce, the Cretaceous Lomas Negra Formation outcrops, containing four limestone beds, cumulatively <3 m thick in a 500 m thick redbed sequence (Marinovic and Lahsen, 1984). Conceivably correlating with this Formation (Charrier and

Reutter, 1994), small inliers of Late Cretaceous-early Paleogene Yacoraite Formation occur >120 km to the SE of El Tatio in Argentina (Rubiolo et al., 2003), and the equivalent Molina Formation some 85 km NE of El Tatio in Bolivia (Pacheco and Ramirez, 1997). Although these may represent a continuous extension of lacustrine/marine conditions underlying the current volcanic arc, both these formations show facies interpreted as lacustrine shorelines (Rohais et al., 2019; Deschamps et al., 2020; Mutti et al., 2023; Villafañe et al., 2023), which might negate any extension to the Loa catchment. The Na-normalized plot of HCO₃:Ca (Figure 5B) does not indicate any significant carbonate in Salado-Toconce baseflow, other than soil/plant CO₂ generation, nor do the HCO₃:Cl and Ca:Cl ratios suggest the presence of deep carbonates (Figures 5viii, 5x). Calcite saturation is attained below the confluence of the Toconce with the Salado at ~3,000 m, but there is no suggestion that this is the result of decarbonation of underlying limestones, so sedimentary limestone is provisionally discounted as a carbonate source.

5.5 Potential structural controls on hydrology

Apart from causing abrupt changes in lithology and related hydraulic properties the impact of faults and folds on groundwater flow and related surface water is poorly known. The inherent anisotropy of fault permeability is commonly associated with a low-*k* core surrounded by a high-*k* damaged zone resulting in reduced cross-flow and enhanced lateral flow (Bense et al., 2013). In this situation there is likely to be a gradient decrease upstream of the fault and increase downstream. Flow nets for the northern aquifers in the Calama Basin (Jordan et al., 2015; Herrera et al., 2021) show this configuration across the West Fissure. Similarly, upstream gradient decrease and downstream increase occurs across the Aquina fault system (Houston, 2006c) that lies between the Lipez-Coranzuli and Calama-Olcapato-El Toro fault systems with the same orientation. The cause of separation between the northern and southern aquifers in the Calama Basin, identified in the lower aquifer hydrochemistry, is unknown, but may be controlled by the monocline or by the combined control of several crustal faults and lineaments (Figure 2).

In addition to horizontal groundwater flow distortions, surface water ponding, and localized base-level revision (incision), there is every reason to suppose that the major faulting systems that control the location of hydrothermal sources (Veloso et al., 2020) also facilitate the vertical ascent of groups II and III type waters. It must also be assumed that open fissures will enhance flow, so that the state of stress will impact groundwater flow. The upper crustal stress regime in northern Chile is variable in space and time. East-west extension dominates current conditions in the Coast Range and forearc but rotates to NE-SW from the Pre-Cordillera eastwards (Lanza et al., 2013; Norini et al., 2013; Tibaldi et al., 2017). However, it is possible that in the short term, changes in hydraulic properties due to earthquake deformation may play an important role in controlling surface and groundwater flow (Ingebritsen and Manga, 2019). Using GPS data Klotz et al. (2001) suggest deformation is dominated by the earthquake cycle which causes compression, followed by rebound in the direction of plate convergence. Furthermore, Scheihing (2023) demonstrates a substantial increase in transient groundwater flow following a 7.8 M_w

earthquake in the forearc, confirming the relevance of seismic activity to surface and groundwater flow.

6 Conclusion

Using an integrated approach to analyze surface water flows, chemistry, and isotopes in the Río Loa catchment during 1999–2000, several storage and flux elements can be recognized. The annual cycle of flood, interflow and baseflow is critical to understanding both flows and chemistry, especially since such elements follow a non-linear cycle over the hydrological year. Baseflow in the Ríos Loa and Salado is overwhelmingly sourced from intra-arc aquifers at >3,000 m, and there is sufficient active storage in these aquifers to maintain perennial baseflow during the long dry season from April to October. These aquifers receive recharge from precipitation infiltration, hydrothermal sources, and it is argued, diffuse upflow from magmatic volatile exsolution and slab dehydration.

Within the Pre-Andean basins there is considerable interaction between the rivers and phreatic aquifers. The complex geology means that aquifer units tend to be somewhat compartmentalized and may be perched, unconfined, semi-confined, or confined and wholly, partially or not-at-all in contact with each other or with surface water and phreatic and perched aquifers as a result of arc volcanism and tectonic activity. Their interactivity with other ground and surface waters is often related to the annual cycle with precipitation and water level/stage acting as controlling factors. Despite river-aquifer exchange there is little evidence for significant additional recharge to the Pre-Andean and forearc aquifers, other than via downstream transfers from upstream sources.

The intra-arc aquifers location, geometry and physico-chemical properties are all inadequately established. Current research tends to be focused on Pre-Andean and forearc aquifers, whereas there is a need for research to be re-focused on these high-altitude intra-arc sources.

Data availability statement

The original contributions presented in the study are included in the article/[Supplementary Material](#), further inquiries can be directed to the corresponding author.

References

- Aguilera, F., Tassi, F., Darrah, T., Moune, S., and Vaselli, O. (2012). Geochemical model of a magmatic–hydrothermal system at the Lastarria volcano, northern Chile. *Bull. Volcanol.* 74, 119–134. doi:10.1007/s00445-011-0489-5
- Aldenderfer, M. S. (1989). The archaic period in the South-Central Andes. *J. World Prehistory* 3, 117–158. doi:10.1007/bf00975759
- A. M. Alonso-Zara and L. H. Tanner (Editors) (2010). *Carbonates in continental settings* (Elsevier).
- Álvarez-Amado, F., Rosales, M., Godfrey, L., Poblete-González, C., Morgado, E., Espinoza, M., et al. (2022). The role of ignimbrites and fine sediments in the lithium distribution and isotopic fractionation in hyperarid environments: insights from Li-isotopes in the Atacama Desert. *J. Geochem. Explor.* 241, 107062. doi:10.1016/j.gexplo.2022.107062
- Álvarez-Campos, O., Olson, E. J., Welp, L. R., Frisbee, M. D., Zúñiga Medina, S. A., Díaz Rodríguez, J., et al. (2022). Evidence for high-elevation salar recharge and

Author contributions

JH: Conception, Implementation and analysis. Writing draft and final.

Funding

The author declares that funding for the flow gauging, chemical and isotopic sampling and analysis program in 1999 and 2000 was provided by Nazca S.A. The funder was not involved in the study design, collection, analysis, interpretation of data, the writing of this article, or the decision to submit it for publication.

Acknowledgments

Thanks to Linda Godfrey for insightful discussions and comments on a previous version. Also to John Harman for reading and critically commenting on an early draft. The DGA are thanked for their help in obtaining the precipitation samples.

Conflict of interest

The author declares that the research was conducted in the absence of any commercial or financial relationships that could be construed as a potential conflict of interest.

Publisher's note

All claims expressed in this article are solely those of the authors and do not necessarily represent those of their affiliated organizations, or those of the publisher, the editors and the reviewers. Any product that may be evaluated in this article, or claim that may be made by its manufacturer, is not guaranteed or endorsed by the publisher.

Supplementary material

The Supplementary Material for this article can be found online at: <https://www.frontiersin.org/articles/10.3389/feart.2023.1310088/full#supplementary-material>

interbasin groundwater flow in the Western Cordillera of the Peruvian Andes. *Hydrology Earth Syst. Sci.* 26 (2), 483–503. doi:10.5194/hess-26-483-2022

Álvarez-Garretón, C., Mendoza, P. A., Boisier, J. P., Addor, N., Galleguillos, M., Zambrano-Bigiarini, M., et al. (2018). The CAMELS-CL dataset: catchment attributes and meteorology for large sample studies—Chile dataset. *Hydrology Earth Syst. Sci.* 22 (11), 5817–5846. doi:10.5194/hess-22-5817-2018

Anderson, M., Low, R., and Foot, S. (2002). Sustainable groundwater development in arid, high Andean basins. *Geol. Soc. Lond. Spec. Publ.* 193 (1), 133–144. doi:10.1144/gsl.sp.2002.193.01.11

Anderson, M. G., and Burt, T. P. (1980). Interpretation of recession flow. *J. Hydrology* 46 (1-2), 89–101. doi:10.1016/0022-1694(80)90037-2

Aravena, R. (1995). Isotope hydrology and geochemistry of northern Chile groundwaters. *Bull. l'Institut français d'études Andin.* 24 (3), 495–503. doi:10.3406/bifea.1995.1200

- Aravena, R., Herrera, C., and Urrutia, J. (2023). *Hydrochemical and isotopic evaluation of groundwater and river water in the transboundary Silala River watershed*. Water: Wiley Interdisciplinary Reviews, e1679. doi:10.1002/wat2.1679
- Aravena, R., and Suzuki, O. (1990). Isotopic evolution of river water in the northern Chile region. *Water Resour. Res.* 26 (12), 2887–2895. doi:10.1029/wr026i012p02887
- Aravena, R., Suzuki, O., Pena, H., Pollastri, A., Fuenzalida, H., and Grilli, A. (1999). Isotopic composition and origin of the precipitation in Northern Chile. *Appl. Geochem.* 14 (4), 411–422. doi:10.1016/S0883-2927(98)00067-5
- Arias, P. A., Garreaud, R., Poveda, G., Espinoza, J. C., Molina-Carpio, J., Masiokas, M., et al. (2021). Hydroclimate of the Andes part II: hydroclimate variability and sub-continental patterns. *Front. Earth Sci.* 8, 666. doi:10.3389/feart.2020.505467
- Barnes, B. S. (1939). The structure of discharge-recession curves. *Eos, Trans. Am. Geophys. Union* 20 (4), 721–725. doi:10.1029/tr020i004p00721
- Barry, P. H., De Moor, J. M., Chiodi, A., Aguilera, F., Hudak, M. R., Bekaert, D. V., et al. (2022). The helium and carbon isotope characteristics of the andean convergent margin. *Front. Earth Sci.* 10, 897267. doi:10.3389/feart.2022.897267
- Basaldúa, A., Alcaraz, E., Quiroz-Londoño, M., Dapeña, C., Ibarra, E., Vélez-Agudelo, C., et al. (2022). Reconstruction of the record of tritium in precipitation in the temperate zone of South America. *Hydrol. Process.* 36 (9), e14691. doi:10.1002/hyp.14691
- Bense, V. F., Gleeson, T., Loveless, S. E., Bour, O., and Scibek, J. (2013). Fault zone hydrogeology. *Earth-Science Rev.* 127, 171–192. doi:10.1016/j.earscirev.2013.09.008
- Bershaw, J., Saylor, J. E., Garziona, C. N., Leier, A., and Sundell, K. E. (2016). Stable isotope variations ($\delta^{18}\text{O}$ and δD) in modern waters across the Andean Plateau. *Geochimica Cosmochimica Acta* 194, 310–324. doi:10.1016/j.gca.2016.08.011
- Bethke, C. M., and Johnson, T. M. (2002). Paradox of groundwater age. *Geology* 30 (2), 107–110. doi:10.1130/0091-7613(2002)030<0107:POGA>2.0.CO;2
- Blanco, N., Tomlinson, A., Mpodozis, C., Pérez de Arce, C., and Matthews, Y. (2003). “Formación Calama, Eoceno, II Región de Antofagasta (Chile): estratigrafía e implicancias tectónicas,” in *Congreso geológico chileno*. 10th (Actas), 10.
- Blanco, N., and Tomlinson, A. J. (2009). *Carta Chiu Chiu: región de Antofagasta*. Servicio Nacional de Geología y Minería.
- Bloomfield, J. P., Bricker, S. H., and Newell, A. J. (2011). Some relationships between lithology, basin form and hydrology: a case study from the Thames basin, UK. *Hydrol. Process.* 25 (16), 2518–2530. doi:10.1002/hyp.8024
- Boers, N., Donner, R. V., Bookhagen, B., and Kurths, J. (2015). Complex network analysis helps to identify impacts of the El Niño Southern Oscillation on moisture divergence in South America. *Clim. Dyn.* 45, 619–632. doi:10.1007/s00382-014-2265-7
- Bougeault, C., Durllet, C., Vennin, E., Muller, E., Ader, M., Ghaleb, B., et al. (2020). Variability of carbonate isotope signatures in a hydrothermally influenced system: insights from the Pastos Grandes Caldera (Bolivia). *Minerals* 10 (11), 989. doi:10.3390/min10110989
- Boutt, D. F., Corenthal, L. G., Moran, B. J., Munk, L., and Hynek, S. A. (2021). Imbalance in the modern hydrologic budget of topographic catchments along the western slope of the Andes (21–25° S): implications for groundwater recharge assessment. *Hydrogeology J.* 29 (3), 985–1007. doi:10.1007/s10040-021-02309-z
- Brown, M., Diaz, F., and Grocott, J. (1993). Displacement history of the Atacama fault system 25°00'S–27°00'S, northern Chile. *Geol. Soc. Am. Bull.* 105 (9), 1165–1174. doi:10.1130/0016-7606(1993)105<1165:dhofat>2.3.co;2
- Cai, W., McPhaden, M. J., Grimm, A. M., Rodrigues, R. R., Taschetto, A. S., Garreaud, R. D., et al. (2020). Climate impacts of the el niño–southern oscillation on south America. *Nat. Rev. Earth Environ.* 1 (4), 215–231. doi:10.1038/s43017-020-0040-3
- Charrier, R., and Reutter, K. J. (1994). “The purilactis group of northern Chile: boundary between arc and backarc from late cretaceous to Eocene,” in *Tectonics of the southern central Andes: structure and evolution of an active continental margin*, 189–202.
- Chen, W. P., and Lee, C. H. (2003). Estimating ground-water recharge from streamflow records. *Environ. Geol.* 44, 257–265. doi:10.1007/s00254-002-0753-2
- Chmielowski, J., Zandt, G., and Haberland, C. (1999). The central Andean Altiplano-Puna magma body. *Geophys. Res. Lett.* 26 (6), 783–786. doi:10.1029/1999GL900078
- Clark, I. (2015). *Groundwater geochemistry and isotopes*. CRC Press. doi:10.1201/b18347
- Corenthal, L. G. (2016). Sources of water and solutes to the salar de Atacama, Chile: a coupled hydrologic, geochemical, and groundwater modeling study. *Masters Theses*. 320. doi:10.7275/7942238
- Cortecchi, G., Boschetti, T., Mussi, M., Lameli, C. H., Mucchino, C., and Barbieri, M. (2005). New chemical and original isotopic data on waters from El Tatío geothermal field, northern Chile. *Geochem. J.* 39 (6), 547–571. doi:10.2343/geochemj.39.547
- de Porras, M. E., Maldonado, A., Hayashida, F. M., Troncoso, A., Salazar, D., Parcero-Oubiña, C., et al. (2021). Socio-environmental dynamics in the central Atacama desert (22°S) during the late Holocene. *Quat. Sci. Rev.* 267, 107097. doi:10.1016/j.quascirev.2021.107097
- Deschamps, R., Rohais, S., Hamon, Y., and Gasparrini, M. (2020). Dynamic of a lacustrine sedimentary system during late rifting at the cretaceous–palaeocene transition: example of the Yacoraite Formation, salta basin, Argentina. *Depositional Rec.* 6 (3), 490–523. doi:10.1002/dep2.116
- De Silva, S. L. (1989). Altiplano-Puna volcanic complex of the central Andes. *Geology* 17 (12), 1102–1106. doi:10.1130/0091-7613(1989)017<1102:apvcot>2.3.co;2
- de Wet, C. B., de Wet, A. P., Godfrey, L., Driscoll, E., Patzkowsky, S., Xu, C., et al. (2020). Pliocene short-term climate changes preserved in continental shallow lacustrine-palustrine carbonates: western Opache Formation, Atacama Desert, Chile. *Geol. Soc. Am. Bull.* 132 (9–10), 1795–1816. doi:10.1130/B35227.1
- de Wet, C. B., Godfrey, L., and de Wet, A. P. (2015). Sedimentology and stable isotopes from a lacustrine-to-palustrine limestone deposited in an arid setting, climatic and tectonic factors: Miocene–Pliocene Opache Formation, Atacama Desert, Chile. *Palaeogeogr. Palaeoclimatol. Palaeoecol.* 426, 46–67. doi:10.1016/j.palaeo.2015.02.039
- Diamond, L. W., Wanner, C., and Waber, H. N. (2018). Penetration depth of meteoric water in orogenic geothermal systems. *Geology* 46 (12), 1063–1066. doi:10.1130/G45394.1
- Dingman, S. L. (1993). *Physical hydrology*. Macmillan.
- Duhart, P., Munoz, J., Quiroz, D., Mestre, A., and Varas, G. (2018). *Carta sierra gorda, región de Antofagasta*. Servicio Nacional de Geología y Minería.
- Espinoza, J. C., Garreaud, R., Poveda, G., Arias, P. A., Molina-Carpio, J., Masiokas, M., et al. (2020). Hydroclimate of the Andes part I: main climatic features. *Front. Earth Sci.* 8, 64. doi:10.3389/feart.2020.00064
- Evenstar, L. A., Hartley, A. J., Archer, S. G., and Neilson, J. E. (2016). Climatic and halokinetic controls on alluvial-lacustrine sedimentation during compressional deformation, Andean forearc, northern Chile. *Basin Res.* 28 (5), 634–657. doi:10.1111/bre.12124
- Faure, G. (1997). *Principles and applications of geochemistry*, 625. Upper Saddle River, NJ: Prentice Hall.
- Ferraris, F. (1978). *Carta tocopilla: región de Antofagasta*. Servicio Nacional de Geología y Minería.
- Fialko, Y., and Pearce, J. (2012). Sombrero uplift above the Altiplano-Puna magma body: evidence of a ballooning mid-crustal diapir. *Science* 338 (6104), 250–252. doi:10.1126/science.1226358
- Fiorella, R. P., Poulsen, C. J., Pillco Zola, R. S., Barnes, J. B., Tabor, C. R., and Ehlers, T. A. (2015). Spatiotemporal variability of modern precipitation $\delta^{18}\text{O}$ in the central Andes and implications for paleoclimate and paleoaltimetry estimates. *J. Geophys. Res. Atmos.* 120 (10), 4630–4656. doi:10.1002/2014JD022893
- Fournier, R. O. (1989). Geochemistry and dynamics of the yellowstone national park hydrothermal system. *Annu. Rev. earth Planet. Sci.* 17 (1), 13–53. doi:10.1146/annurev.ea.17.050189.000305
- Frisbee, M. D., Tolley, D. G., and Wilson, J. L. (2017). Field estimates of groundwater circulation depths in two mountainous watersheds in the western US and the effect of deep circulation on solute concentrations in streamflow. *Water Resour. Res.* 53 (4), 2693–2715. doi:10.1002/2016WR019553
- Gaillardet, J., Dupré, B., Louvat, P., and Allegre, C. J. (1999). Global silicate weathering and CO₂ consumption rates deduced from the chemistry of large rivers. *Chem. Geol.* 159 (1–4), 3–30. doi:10.1016/S0009-2541(99)00031-5
- Garreaud, R., Vuille, M., and Clement, A. C. (2003). The climate of the Altiplano: observed current conditions and mechanisms of past changes. *Palaeogeogr. Palaeoclimatol. Palaeoecol.* 194 (1–3), 5–22. doi:10.1016/S0031-0182(03)00269-4
- Garreaud, R. D., Vuille, M., Compagnucci, R., and Marengo, J. (2009). Present-day South American climate. *Palaeogeography, Palaeoclimatology, Palaeoecology*. 281 (3–4), 180–195. doi:10.1016/j.palaeo.2007.10.032
- Garziona, C. N., McQuarrie, N., Perez, N. D., Ehlers, T. A., Beck, S. L., Kar, N., et al. (2017). Tectonic evolution of the Central Andean plateau and implications for the growth of plateaus. *Annu. Rev. Earth Planet. Sci.* 45, 529–559. doi:10.1146/annurev-earth-063016-020612
- Gat, J. R. (2010). *Isotope hydrology: a study of the water cycle*, 6. Imperial College Press.
- Gayo, E. M., Latorre, C., Jordan, T. E., Nester, P. L., Estay, S. A., Ojeda, K. F., et al. (2012). Late Quaternary hydrological and ecological changes in the hyperarid core of the northern Atacama Desert (~21° S). *Earth-Science Rev.* 113 (3–4), 120–140. doi:10.1016/j.earscirev.2012.04.003
- Giggenbach, W. F. (1978). The isotopic composition of waters from the El Tatío geothermal field, Northern Chile. *Geochimica Cosmochimica Acta* 42 (7), 979–988. doi:10.1016/0016-7037(78)90287-9
- Giggenbach, W. F. (1992). Isotopic shifts in waters from geothermal and volcanic systems along convergent plate boundaries and their origin. *Earth Planet. Sci. Lett.* 113 (4), 495–510. doi:10.1016/0012-821X(92)90127-H
- Godfrey, L. V., Herrera, C., Burr, G. S., Houston, J., Aguirre, I., and Jordan, T. E. (2021). $\delta^{13}\text{C}$ and ^{14}C activity of groundwater DOC and DIC in the volcanically active and arid Loa Basin of northern Chile. *J. Hydrology* 595, 125987. doi:10.1016/j.jhydrol.2021.125987
- Godfrey, L. V., Herrera, C., Gamboa, C., and Mathur, R. (2019). Chemical and isotopic evolution of groundwater through the active Andean arc of Northern Chile. *Chem. Geol.* 518, 32–44. doi:10.1016/j.chemgeo.2019.04.011
- Godoy, B., and Kojima, S. (2013). *Structural control on magmatic evolution of san pedro-linzor volcanic chain, central Andes, northern Chile*. Vina del Mar: Congreso Geológico Chileno.

- Godoy, B., Lazcano, J., Rodríguez, I., Martínez, P., Parada, M. A., Le Roux, P., et al. (2018). Geological evolution of Paniri volcano, central Andes, northern Chile. *J. S. Am. Earth Sci.* 84, 184–200. doi:10.1016/j.jsames.2018.03.013
- Godoy, B., Taussi, M., González-Maurel, O., Hübner, D., Lister, J., Sellés, D., et al. (2022). Evolution of the Azufre volcano (northern Chile): implications for the Cerro Pabellón Geothermal Field as inferred from long lasting eruptive activity. *J. Volcanol. Geotherm. Res.* 423, 107472. doi:10.1016/j.jvolgeores.2022.107472
- Godoy, B., Wörner, G., Kojima, S., Aguilera, F., Simon, K., and Hartmann, G. (2014). Low-pressure evolution of arc magmas in thickened crust: the San Pedro–Linzor volcanic chain, Central Andes, northern Chile. *J. S. Am. earth Sci.* 52, 24–42. doi:10.1016/j.jsames.2014.02.004
- Godoy, B., Wörner, G., Le Roux, P., de Silva, S., Parada, M. A., Kojima, S., et al. (2017). Sr-And Nd-isotope variations along the Pleistocene san pedro–linzor volcanic chain, N. Chile: tracking the influence of the upper crustal altiplano-puna magma body. *J. Volcanol. Geotherm. Res.* 341, 172–186. doi:10.1016/j.jvolgeores.2017.05.030
- Goff, F., and McMurtry, G. M. (2000). Tritium and stable isotopes of magmatic waters. *J. Volcanol. Geotherm. Res.* 97 (1–4), 347–396. doi:10.1016/S0377-0273(99)00177-8
- González-Maurel, O., Deegan, F. M., Le Roux, P., Harris, C., Troll, V. R., and Godoy, B. (2020). Constraining the sub-arc, parental magma composition for the giant Altiplano-Puna Volcanic Complex, northern Chile. *Sci. Rep.* 10 (1), 6864–6910. doi:10.1038/s41598-020-63454-1
- González-Maurel, O., Godoy, B., Le Roux, P., Rodríguez, I., Marin, C., Menzies, A., et al. (2019). Magmatic differentiation at La Poruña scoria cone, Central Andes, northern Chile: evidence for assimilation during turbulent ascent processes, and genetic links with mafic eruptions at adjacent San Pedro volcano. *Lithos* 338, 128–140. doi:10.1016/j.lithos.2019.03.033
- González-Pinilla, F. J., Latorre, C., Rojas, M., Houston, J., Rocuant, M. I., Maldonado, A., et al. (2021). High- and low-latitude forcings drive Atacama Desert rainfall variations over the past 16,000 years. *Sci. Adv.* 7 (38), eabg1333. doi:10.1126/sciadv.abg1333
- Gottsmann, J., Eiden, E., and Pritchard, M. E. (2022). Transcrustal compressible fluid flow explains the altiplano-puna gravity and deformation anomalies. *Geophys. Res. Lett.* 49 (16), e2022GL099487. doi:10.1029/2022GL099487
- Hack, A. C., and Thompson, A. B. (2011). Density and viscosity of hydrous magmas and related fluids and their role in subduction zone processes. *J. Petrology* 52 (7–8), 1333–1362. doi:10.1093/petrology/egg048
- Hall, F. R. (1968). Base-flow recessions—a review. *Water Resour. Res.* 4 (5), 973–983. doi:10.1029/WR004i005p0973
- Hartley, A. J., and Evenstar, L. (2010). Cenozoic stratigraphic development in the north Chilean forearc: implications for basin development and uplift history of the Central Andean margin. *Tectonophysics* 495 (1–2), 67–77. doi:10.1016/j.tecto.2009.05.013
- Herrera, C., Godfrey, L., Urrutia, J., Custodio, E., Jordan, T., Jódar, J., et al. (2021). Recharge and residence times of groundwater in hyper arid areas: the confined aquifer of Calama, Loa River Basin, Atacama Desert, Chile. *Sci. Total Environ.* 752, 141847. doi:10.1016/j.scitotenv.2020.141847
- Hoke, G. D., Isacks, B. L., Jordan, T. E., Blanco, N., Tomlinson, A. J., and Ramezani, J. (2007). Geomorphic evidence for post-10 Ma uplift of the western flank of the central Andes 18°30′–22°S. *Tectonics* 26 (5). doi:10.1029/2006TC002082
- Hoke, L., Hilton, D. R., Lamb, S. H., Hammerschmidt, K., and Friedrichsen, H. (1994). 3He evidence for a wide zone of active mantle melting beneath the Central Andes. *Earth Planet. Sci. Lett.* 128 (3–4), 341–355. doi:10.1016/0012-821X(94)90155-4
- Hornbeck, J. W. (1986). “Modelling the accumulation and effects of chemicals in snow,” in *Modelling snowmelt-induced processes. Proceedings of the IAHS Budapest symposium*, 325–333.
- Horton, B. K. (2018). Sedimentary record of Andean mountain building. *Earth-Science Rev.* 178, 279–309. doi:10.1016/j.earscirev.2017.11.025
- Horton, R. E. (1933). The role of infiltration in the hydrologic cycle. *Eos, Trans. Am. Geophys. Union* 14 (1), 446–460. doi:10.1029/TR014i001p00446
- Houston, J. (2002). Groundwater recharge through an alluvial fan in the Atacama Desert, northern Chile: mechanisms, magnitudes and causes. *Hydrol. Process.* 16 (15), 3019–3035. doi:10.1002/hyp.1086
- Houston, J. (2004). High-resolution sequence stratigraphy as a tool in hydrogeological exploration in the Atacama Desert. *Q. J. Eng. Geol. Hydrogeology* 37 (1), 7–17. doi:10.1144/1470-9236/03-013
- Houston, J. (2005). The great Atacama flood of 2001 and its implications for Andean hydrology. *Hydrological Process. An Int. J.* 20 (3), 591–610. doi:10.1002/hyp.5926
- Houston, J. (2006a). Evaporation in the Atacama Desert: an empirical study of spatio-temporal variations and their causes. *J. Hydrology* 330 (3–4), 402–412. doi:10.1016/j.jhydrol.2006.03.036
- Houston, J. (2006b). Variability of precipitation in the Atacama Desert: its causes and hydrological impact. *Int. J. Climatol. A J. R. Meteorological Soc.* 26 (15), 2181–2198. doi:10.1002/joc.1359
- Houston, J. (2006c). Recharge to groundwater in the Turi Basin, northern Chile: an evaluation based on tritium and chloride mass balance techniques. *J. Hydrology* 334 (3–4), 534–544. doi:10.1016/j.jhydrol.2006.10.030
- Houston, J. (2009). A recharge model for high altitude, arid, Andean aquifers. *Hydrological Process. An Int. J.* 23 (16), 2383–2393. doi:10.1002/hyp.7350
- Houston, J., and Hartley, A. J. (2003). The central Andean west-slope rainshadow and its potential contribution to the origin of hyper-aridity in the Atacama Desert. *Int. J. Climatol. A J. R. Meteorological Soc.* 23 (12), 1453–1464. doi:10.1002/joc.938
- Houston, J., Iglesias, A. J., and Cunich, G. A. (2001). Constitución de derechos de aprovechamiento sobre aguas subterráneas almacenadas. *Rev. Derecho Adm. Económico* (5), 117–127. doi:10.7764/redae.5.4
- Houston, J., and Latorre, C. (2022). The role of the non-stationary Andean Dry Diagonal in paleoclimate reconstructions. *Hydrol. Process.* 36 (10), e14723. doi:10.1002/hyp.14723
- Hovland, M., Rueslåtten, H., and Johnsen, H. K. (2018a). Large salt accumulations as a consequence of hydrothermal processes associated with ‘Wilson cycles’: a review Part 1: towards a new understanding. *Mar. Petroleum Geol.* 92, 987–1009. doi:10.1016/j.marpetgeo.2017.12.029
- Hovland, M., Rueslåtten, H., and Johnsen, H. K. (2018b). Large salt accumulations as a consequence of hydrothermal processes associated with ‘Wilson cycles’: a review, Part 2: application of a new salt-forming model on selected cases. *Mar. Petroleum Geol.* 92, 128–148. doi:10.1016/j.marpetgeo.2018.02.015
- Hudson, T. S., Kendall, J. M., Pritchard, M. E., Blundy, J. D., and Gottsmann, J. H. (2022). From slab to surface: earthquake evidence for fluid migration at Uturuncu volcano, Bolivia. *Earth Planet. Sci. Lett.* 577, 117268. doi:10.1016/j.epsl.2021.117268
- Ibarra, F., and Prezzi, C. B. (2019). The thermo-mechanical state of the andes in the Altiplano-Puna region: insights from curie isotherm and effective elastic thickness determination. *Rev. Asoc. Geol. Argent.* 76 (4), 352–362.
- Ingebritsen, S. E., and Manga, M. (2019). Earthquake hydrogeology. *Water Resour. Res.* 55 (7), 5212–5216. doi:10.1029/2019WR025341
- Ingebritsen, S. E., and Manning, C. E. (2002). Diffuse fluid flux through orogenic belts: implications for the world ocean. *Proc. Natl. Acad. Sci.* 99 (14), 9113–9116. doi:10.1073/pnas.132275699
- Jayne, R. S., Pollyea, R. M., Dodd, J. P., Olson, E. J., and Swanson, S. K. (2016). Spatial and temporal constraints on regional-scale groundwater flow in the Pampa del Tamarugal Basin, Atacama Desert, Chile. *Hydrogeology J.* 24 (8), 1921–1937. doi:10.1007/s10040-016-1454-3
- Jensen, P. A. I. (1992). *Las cuencas aluvio-lacustres oligoceno-neogenas de la region de ante-arco de Chile septentrional, entre los 19 grados y 23 grados sur*. PhD Thesis. Universidad de Barcelona.
- JICA (1995). *The study on the development of water resources in northern Chile*. Dirección General de Aguas: Japan International Cooperation Agency (JICA), Ministerio de Obras Públicas.
- Jordan, T., Lameli, C. H., Kirk-Lawlor, N., and Godfrey, L. (2015). Architecture of the aquifers of the Calama Basin, Loa catchment basin, northern Chile. *Geosphere* 11 (5), 1438–1474. doi:10.1130/GES01176.1
- Jordan, T., Quezada, A., Blanco, N., Jensen, A., Vásquez, P., and Sepúlveda, F. (2022). Paleoenvironmental evolution of a forearc in response to forcings by drainage, climate, volcanism, and tectonics: the Quillagua depocenter, Chile. *Lithosphere* 2022 (1), 1024844. doi:10.2113/2022/1024844
- Jordan, T. E., Muñoz, N., Hein, M., Lowenstein, T., Godfrey, L., and Yu, J. (2002). Active faulting and folding without topographic expression in an evaporite basin, Chile. *GSA Bull.* 114 (11), 1406–1421. doi:10.1130/0016-7606(2002)114<1406:afawt>2.0.co;2
- Jordan, T. E., Nester, P. L., Blanco, N., Hoke, G. D., Dávila, F., and Tomlinson, A. J. (2010). Uplift of the Altiplano-Puna plateau: a view from the west. *Tectonics* 29 (5). doi:10.1029/2010TC002661
- Klotz, J., Khazaradze, G., Angermann, D., Reigber, C., Perdomo, R., and Cifuentes, O. (2001). Earthquake cycle dominates contemporary crustal deformation in Central and Southern Andes. *Earth Planet. Sci. Lett.* 193 (3–4), 437–446. doi:10.1016/S0012-821X(01)00532-5
- Lamb, S. (2016). Cenozoic uplift of the Central Andes in northern Chile and Bolivia—reconciling paleoaltimetry with the geological evolution. *Can. J. Earth Sci.* 53 (11), 1227–1245. doi:10.1139/cjes-2015-0071
- Lanza, F., Tibaldi, A., Bonali, F. L., and Corazzato, C. (2013). Space–time variations of stresses in the miocene–quaternary along the calama–olacapato–el Toro fault Zone, central andes. *Tectonophysics* 593, 33–56. doi:10.1016/j.tecto.2013.02.029
- Latorre, C., Betancourt, J. L., Rylander, K. A., and Quade, J. (2002). Vegetation invasions into absolute desert: a 45;th000 yr rodent midden record from the Calama–Salar de Atacama basins, northern Chile (lat 22°–24°S). *Geol. Soc. Am. Bull.* 114 (3), 349–366. doi:10.1130/0016-7606(2002)114<0349:viada>2.0.co;2
- Latorre, C., Santoro, C. M., Ugalde, P. C., Gayo, E. M., Osorio, D., Salas-Egaña, C., et al. (2013). Late Pleistocene human occupation of the hyperarid core in the Atacama Desert, northern Chile. *Quat. Sci. Rev.* 77, 19–30. doi:10.1016/j.quascirev.2013.06.008
- Laumonier, M., Gaillard, F., Muir, D., Blundy, J., and Unsworth, M. (2017). Giant magmatic water reservoirs at mid-crustal depth inferred from electrical conductivity and the growth of the continental crust. *Earth Planet. Sci. Lett.* 457, 173–180. doi:10.1016/j.epsl.2016.10.023

- Lenters, J. D., and Cook, K. H. (1997). On the origin of the Bolivian high and related circulation features of the South American climate. *J. Atmos. Sci.* 54 (5), 656–678. doi:10.1175/1520-0469(1997)054<0656:ootob>2.0.co;2
- Letelier, J. A., O'Sullivan, J., Reich, M., Veloso, E., Sánchez-Alfaro, P., Aravena, D., et al. (2021). Reservoir architecture model and heat transfer modes in the El Tatio-La Torta geothermal system, Central Andes of northern Chile. *Geothermics* 89, 101940. doi:10.1016/j.geothermics.2020.101940
- López, C., Martínez, F., Del Ventisette, C., Bonini, M., Montanari, D., Muñoz, B., et al. (2020). East-vergent thrusts and inversion structures: an updated tectonic model to understand the Domeyko Cordillera and the Salar de Atacama Basin transition in the western Central Andes. *J. S. Am. Earth Sci.* 103, 102741. doi:10.1016/j.jsames.2020.102741
- Magaritz, M., Aravena, R., Peña, H., Suzuki, O., and Grilli, A. (1989). Water chemistry and isotope study of streams and springs in northern Chile. *J. Hydrology* 108, 323–341. doi:10.1016/0022-1694(89)90292-8
- Magaritz, M., Aravena, R., Peña, H., Suzuki, O., and Grilli, A. (1990). Source of ground water in the deserts of northern Chile: evidence of deep circulation of ground water from the Andes. *Groundwater* 28 (4), 513–517. doi:10.1111/j.1745-6584.1990.tb01706.x
- Mancini, R., Díaz, D., Brasse, H., Godoy, B., and Hernández, M. J. (2019). Conductivity distribution beneath the San Pedro-Linzor volcanic chain, North Chile, using 3-D magnetotelluric modeling. *J. Geophys. Res. Solid Earth* 124 (5), 4386–4398. doi:10.1029/2018JB016114
- Manning, C. E., and Ingebritsen, S. E. (1999). Permeability of the continental crust: implications of geothermal data and metamorphic systems. *Rev. Geophys.* 37 (1), 127–150. doi:10.1029/1998RG900002
- Marín, C., Rodríguez, I., Godoy, B., González-Maurel, O., Le Roux, P., Medina, E., et al. (2020). Eruptive history of La Poruña scoria cone, central andes, northern Chile. *Bull. Volcanol.* 82, 74–19. doi:10.1007/s00445-020-01410-7
- Marinović, N., and Lahsen, A. (1984). *Hoja Calama, región de Antofagasta: escala 1:250.000*. Servicio Nacional de Geología y Minería.
- May, G., Hartley, A. J., Chong, G., Stuart, F., Turner, P., and Kape, S. J. (2005). Eocene to Pleistocene lithostratigraphy, chronostratigraphy and tectono-sedimentary evolution of the Calama Basin, northern Chile. *Rev. Geol. Chile* 32 (1), 33–58. doi:10.4067/S0716-02082005000100003
- May, G., Hartley, A. J., Stuart, F. M., and Chong, G. (1999). Tectonic signatures in arid continental basins: an example from the Upper Miocene–Pleistocene, Calama Basin, Andean forearc, northern Chile. *Palaeogeogr. Palaeoclimatol. Palaeoecol.* 151 (1–3), 55–77. doi:10.1016/S0031-0182(99)00016-4
- Medina, E., Jensen, A., Niemyer, H., Wilke, H., Cembrano, J., Garcia, M., et al. (2012). *Cartas tocopilla y maria elena, region de Antofagasta*. Servicio Nacional de Geología y Minería.
- Meyboom, P. (1961). Estimating ground-water recharge from stream hydrographs. *J. Geophys. Res.* 66 (4), 1203–1214. doi:10.1029/JZ066i004p01203
- Mohren, J., Binnie, S. A., Ritter, B., and Dunai, T. J. (2020). Development of a steep erosional gradient over a short distance in the hyperarid core of the Atacama Desert, northern Chile. *Glob. Planet. Change* 184, 103068. doi:10.1016/j.gloplacha.2019.103068
- Montecinos-Cuadros, D., Díaz, D., Yogeshwar, P., and Munoz-Saez, C. (2021). Characterization of the shallow structure of El Tatio geothermal field in the Central Andes, Chile using transient electromagnetics. *J. Volcanol. Geotherm. Res.* 412, 107198. doi:10.1016/j.jvolgeores.2021.107198
- Montgomery, E. L., Rosko, M. J., Castro, S. O., Keller, B. R., and Bevacqua, P. S. (2003). Interbasin underflow between closed Altiplano basins in Chile. *Groundwater* 41 (4), 523–531. doi:10.1111/j.1745-6584.2003.tb02386.x
- Moran, B. J., Boutt, D. F., and Munk, L. A. (2019). Stable and radioisotope systematics reveal fossil water as fundamental characteristic of arid orogenic-scale groundwater systems. *Water Resour. Res.* 55 (12), 11295–11315. doi:10.1029/2019WR026386
- Morata, D., Maza, S. N., Vidal, J., Taussi, M., Renzulli, A., Mattioli, M., et al. (2020). “Hydrothermal alteration in Cerro pabellón geothermal field: from surface and drill core data to conceptual model,” in *Proceedings of the world geothermal congress, Reykjavik, Iceland*, 1.
- Moreno, A., Santoro, C. M., and Latorre, C. (2009). Climate change and human occupation in the northernmost Chilean Altiplano over the last ca. 11 500 cal. a BP. *J. Quat. Sci.* 24 (4), 373–382. doi:10.1002/jqs.1240
- Mpodozis, C., Arriagada, C., Basso, M., Roperch, P., Cobbold, P., and Reich, M. (2005). Late mesozoic to Paleogene stratigraphy of the salar de Atacama basin, Antofagasta, northern Chile: implications for the tectonic evolution of the central andes. *Tectonophysics* 399 (1–4), 125–154. doi:10.1016/j.tecto.2004.12.019
- Muller, E., Gaucher, E. C., Durllet, C., Moquet, J. S., Moreira, M., Rouchon, V., et al. (2020). The origin of continental carbonates in Andean salars: a multi-tracer geochemical approach in Laguna Pastos Grandes (Bolivia). *Geochimica Cosmochimica Acta* 279, 220–237. doi:10.1016/j.gca.2020.03.020
- Munk, L. A., Boutt, D. F., Hynek, S. A., and Moran, B. J. (2018). Hydrogeochemical fluxes and processes contributing to the formation of lithium-enriched brines in a hyper-arid continental basin. *Chem. Geol.* 493, 37–57. doi:10.1016/j.chemgeo.2018.05.013
- Muñoz, J. F., Suárez, F., Alcayaga, H., McRostie, V., and Fernández, B. (2023). *Introduction to the Silala river and its hydrology*. Water: Wiley Interdisciplinary Reviews, e1644. doi:10.1002/wat2.1644
- Munoz-Saez, C., Manga, M., and Hurwitz, S. (2018). Hydrothermal discharge from the el Tatio basin, Atacama, Chile. *J. Volcanol. Geotherm. Res.* 361, 25–35. doi:10.1016/j.jvolgeores.2018.07.007
- Mutti, M., Vallati, M., Tomás, S., Galli, C., Rumbelsperger, A. M. B., Maerz, S., et al. (2023). Constraining depositional evolution and reservoir compartmentalization in a mixed carbonate-siliciclastic lacustrine system: the Yacoraita formation, Salta Group, NW Argentina. *Mar. Petroleum Geol.* 149, 106049. doi:10.1016/j.marpetgeo.2022.106049
- Naranjo, J. A., and Paskoff, R. P. (1982). *Estratigrafía de las unidades sedimentarias cenozoicas de la cuenca del Río Loa en la Pampa del Tamarugal, Región de Antofagasta, Chile*. Revista Geológica de Chile. No. 15.
- Nester, P. L., Gayo, E., Latorre, C., Jordan, T. E., and Blanco, N. (2007). Perennial stream discharge in the hyperarid Atacama Desert of northern Chile during the latest Pleistocene. *Proc. Natl. Acad. Sci.* 104 (50), 19724–19729. doi:10.1073/pnas.0705373104
- Norini, G., Baez, W., Becchio, R., Viramonte, J., Giordano, G., Arnosio, M., et al. (2013). The calama-olacapato-el Toro fault system in the Puna plateau, central andes: geodynamic implications and stratovolcanoes emplacement. *Tectonophysics* 608, 1280–1297. doi:10.1016/j.tecto.2013.06.013
- Núñez, L., and Grosjean, M. (2003). “Biodiversity and human impact during the last 11,000 years in North-Central Chile,” in *How landscapes change: human disturbance and ecosystem fragmentation in the americas*, 7–17. doi:10.1007/978-3-662-05238-9_2
- Pacheco, J., and Ramírez, V. (1997). *Mapa geológico de Cañapa/alota hoja 5929/6029*. Carta geológica de Bolivia.
- Palacios, C., Ramírez, L. E., Townley, B., Solari, M., and Guerra, N. (2007). The role of the Antofagasta–Calama Lineament in ore deposit deformation in the Andes of northern Chile. *Miner. Deposita* 42, 301–308. doi:10.1007/s00126-006-0113-3
- Parkhurst, D. L., and Appelo, C. A. J. (2013). Description of input and examples for PHREEQC version 3—a computer program for speciation, batch-reaction, one-dimensional transport, and inverse geochemical calculations. *U. S. Geol. Surv. Tech. methods* 6 (A43), 497.
- Peach, D., and Taylor, A. (2023). *The development of a hydrogeological conceptual model of groundwater and surface water flows in the Silala River Basin*. Water: Wiley Interdisciplinary Reviews, e1676. doi:10.1002/wat2.1676
- Pestle, W. J., Torres-Rouff, C., Gallardo, F., Ballester, B., and Clarot, A. (2015). Mobility and exchange among marine hunter-gatherer and agropastoralist communities in the Formative Period Atacama Desert. *Curr. Anthropol.* 56 (1), 121–133. doi:10.1086/679594
- Poveda, G., Espinoza, J. C., Zuluaga, M. D., Solman, S. A., Garreaud, R., and Van Oevelen, P. J. (2020). High impact weather events in the Andes. *Front. Earth Sci.* 8, 162. doi:10.3389/feart.2020.00162
- Pritchard, M. E., De Silva, S. L., Michelfelder, G., Zandt, G., McNutt, S. R., Gottsmann, J., et al. (2018). Synthesis: PLUTONS: investigating the relationship between pluton growth and volcanism in the Central Andes. *Geosphere* 14 (3), 954–982. doi:10.1130/GES01578.1
- Rech, J. A., Quade, J., and Hart, W. S. (2003). Isotopic evidence for the source of Ca and S in soil gypsum, anhydrite and calcite in the Atacama Desert, Chile. *Geochimica Cosmochimica Acta* 67 (4), 575–586. doi:10.1016/S0016-7037(02)01175-4
- Reutter, K. J., Chong, G., and Scheuber, E. (1993). The “West Fissure” and the Precordillera fault system of northern Chile. *ORSTOM ISAG*, 237–240.
- Risacher, F., Alonso, H., and Salazar, C. (2003). The origin of brines and salts in Chilean salars: a hydrochemical review. *Earth-Science Rev.* 63 (3–4), 249–293. doi:10.1016/S0012-8252(03)00037-0
- Risacher, F., and Fritz, B. (1991). Geochemistry of Bolivian salars, Lipez, southern Altiplano: origin of solutes and brine evolution. *Geochimica Cosmochimica Acta* 55 (3), 687–705. doi:10.1016/0016-7037(91)90334-2
- Risacher, F., Fritz, B., and Hauser, A. (2011). Origin of components in Chilean thermal waters. *J. S. Am. Earth Sci.* 31 (1), 153–170. doi:10.1016/j.jsames.2010.07.002
- Rissmann, C., Leybourne, M., Benn, C., and Christenson, B. (2015). The origin of solutes within the groundwaters of a high Andean aquifer. *Chem. Geol.* 396, 164–181. doi:10.1016/j.chemgeo.2014.11.029
- Rohais, S., Hamon, Y., Deschamps, R., Beaumont, V., Gasparrini, M., Pillot, D., et al. (2019). Patterns of organic carbon enrichment in a lacustrine system across the KT boundary: insight from a multi-proxy analysis of the Yacoraita Formation, Salta rift basin, Argentina. *Int. J. Coal Geol.* 210, 103208. doi:10.1016/j.coal.2019.05.015
- Rojas, R., Batelaan, O., Feyen, L., and Dassargues, A. (2010). Assessment of conceptual model uncertainty for the regional aquifer Pampa del Tamarugal–North Chile. *Hydrology Earth Syst. Sci.* 14 (2), 171–192. doi:10.5194/hess-14-171-2010
- Rorabaugh, M. I. (1964). Estimating changes in bank storage and ground-water contribution to streamflow. *Int. Assoc. Sci. Hydrology Publ.* 63, 432–441.
- Rubiolo, D., Gallardo, E., Disalvo, A., Sánchez, M. C., Turel, A. V., Seggiaro, R. E., et al. (2003). *Hoja geológica 2366-II/2166-IV La quiaca*.
- Sáez, A., Cabrera, L., Garcés, M., van den Bogaard, P., Jensen, A., and Gimeno, D. (2012). The stratigraphic record of changing hyperaridity in the Atacama desert over the last 10 Ma. *Earth Planet. Sci. Lett.* 355, 32–38. doi:10.1016/j.epsl.2012.08.029

- Sáez, A., Cabrera, L., Jensen, A., and Chong, G. (1999). Late Neogene lacustrine record and palaeogeography in the Quillagua–Llamara basin, Central Andean fore-arc (northern Chile). *Palaeogeogr. Palaeoclimatol. Palaeoecol.* 151 (1–3), 5–37. doi:10.1016/S0031-0182(99)00013-9
- Samuel, A., Blin, N., Muñoz, J. F., and Suárez, F. (2019). An unsaturated/saturated coupled hydrogeological model for the Llamara salt flat, Chile, to investigate *Prosopis tamarugo* survival. *Geosciences* 10 (1), 1. doi:10.3390/geosciences10010001
- Scandiffio, G., and Alvarez, M. (1992). *Geochemical report on the Laguna Colorada geothermal area*. Bolivia. No. IAEA-TECDOC-641.
- Scheihing, K. W. (2023). Post-seismic mountain aquifer leakage drives multi-annual forearc basin recharge in the Atacama Desert. *Hydrological Sci. J.* 68 (1), 49–61. doi:10.1080/02626667.2022.2147011
- Scheihing, K. W., Moya, C. E., Struck, U., Licteuvot, E., and Tröger, U. (2017). Reassessing hydrological processes that control stable isotope tracers in groundwater of the Atacama Desert (Northern Chile). *Hydrology* 5 (1), 3. doi:10.3390/hydrology5010003
- Schurr, B., Asch, G., Rietbrock, A., Trumbull, R., and Haberland, C. (2003). Complex patterns of fluid and melt transport in the central Andean subduction zone revealed by attenuation tomography. *Earth Planet. Sci. Lett.* 215 (1–2), 105–119. doi:10.1016/S0012-821X(03)00441-2
- Singh, K. P., and Stall, J. B. (1971). Derivation of base flow recession curves and parameters. *Water Resour. Res.* 7 (2), 292–303. doi:10.1029/WR007i02p0292
- Skarmeta, J., and Marinovic, N. (1981). *Geología de la Hoja Quillagua. Región de Antofagasta*. Escala 1: 250.000.
- Sodoudi, F., Yuan, X., Asch, G., and Kind, R. (2011). High-resolution image of the geometry and thickness of the subducting Nazca lithosphere beneath northern Chile. *J. Geophys. Res. Solid Earth* 116 (B4), B04302. doi:10.1029/2010JB007829
- Somers, L. D., and McKenzie, J. M. (2020). A review of groundwater in high mountain environments. *Wiley Interdiscip. Rev. Water* 7 (6), e1475. doi:10.1002/wat2.1475
- Sparks, R. S. J., Folkes, C. B., Humphreys, M. C., Barford, D. N., Clavero, J., Sunagua, M. C., et al. (2008). Uturuncu volcano, Bolivia: volcanic unrest due to mid-crustal magma intrusion. *Am. J. Sci.* 308 (6), 727–769. doi:10.2475/06.2008.01
- Stoelzle, M., Schuetz, T., Weiler, M., Stahl, K., and Tallaksen, L. M. (2020). Beyond binary baseflow separation: a delayed-flow index for multiple streamflow contributions. *Hydrology Earth Syst. Sci.* 24 (2), 849–867. doi:10.5194/hess-24-849-2020
- Suárez, F., Sarabia, A., Sanzana, P., Latorre, C., and Muñoz, J. F. (2023). *The Quebrada Negra wetland study: an approach to understand plant diversity, hydrology, and hydrogeology of high-Andean wetlands*. Wiley Interdisciplinary Reviews: Water, e1683. doi:10.1002/wat2.1683
- Sujono, J., Shikasho, S., and Hiramatsu, K. (2004). A comparison of techniques for hydrograph recession analysis. *Hydrol. Process.* 18 (3), 403–413. doi:10.1002/hyp.1247
- Sullcani, P. R. R. (2015). *Well data analysis and volumetric assessment of the sol de mañana geothermal field*. Bolivia: United Nations University. Report No. 30.
- Sun, L., Wang, H., and Liu, F. (2019). Combined effect of the QBO and ENSO on the MJO. *Atmos. Ocean. Sci. Lett.* 12 (3), 170–176. doi:10.1080/16742834.2019.1588064
- Szilágyi, J., Parlange, M. B., and Albertson, J. D. (1998). Recession flow analysis for aquifer parameter determination. *Water Resour. Res.* 34 (7), 1851–1857. doi:10.1029/98WR01009
- Takahashi, K., Montecinos, A., Goubanova, K., and Dewitte, B. (2011). ENSO regimes: reinterpreting the canonical and modoki el Niño. *Geophys. Res. Lett.* 38 (10). doi:10.1029/2011GL047364
- Tallaksen, L. M. (1995). A review of baseflow recession analysis. *J. hydrology* 165 (1–4), 349–370. doi:10.1016/0022-1694(94)02540-R
- Tapia, J., Schneider, B., Inostroza, M., Álvarez-Amado, F., Luque, J. A., Aguilera, F., et al. (2021). Naturally elevated arsenic in the Altiplano-Puna, Chile and the link to recent (Mio-Pliocene to Quaternary) volcanic activity, high crustal thicknesses, and geological structures. *J. S. Am. Earth Sci.* 105, 102905. doi:10.1016/j.jsames.2020.102905
- Taussi, M., Nisi, B., Vaselli, O., Maza, S., Morata, D., and Renzulli, A. (2021). Soil CO₂ flux and temperature from a new geothermal area in the Cordón de Inacaliri Volcanic Complex (northern Chile). *Geothermics* 89, 101961. doi:10.1016/j.geothermics.2020.101961
- Tibaldi, A., Bonali, F. L., and Corazzato, C. (2017). Structural control on volcanoes and magma paths from local-to orogen-scale: the central Andes case. *Tectonophysics* 699, 16–41. doi:10.1016/j.tecto.2017.01.005
- Tomlinson, A. J., Blanco, N., Dilles, J. H., Maksaev, V., and Ladino, M. (2010). Carta Calama, Región de Antofagasta. Carta Geológica de Chile, Serie Preliminar. *Serv. Nac. Geol. Minería* 8 (3).
- Tóth, J. (2009). *Gravitational systems of groundwater flow: theory, evaluation, utilization*. Cambridge University Press. doi:10.1017/CBO9780511576546
- Troch, P. A., Berne, A., Bogaart, P., Harman, C., Hilberts, A. G., Lyon, S. W., et al. (2013). The importance of hydraulic groundwater theory in catchment hydrology: the legacy of Wilfried Brutsaert and Jean-Yves Parlange. *Water Resour. Res.* 49 (9), 5099–5116. doi:10.1002/wrcr.20407
- Tucker, M. E., and Wright, V. P. (1990). *Carbonate sedimentology*. John Wiley & Sons.
- Tully, C. D., Rech, J. A., Workman, T. R., Santoro, C. M., Capriles, J. M., Gayo, E. M., et al. (2019). In-stream wetland deposits, megadroughts, and cultural change in the northern Atacama Desert, Chile. *Quat. Res.* 91 (1), 63–80. doi:10.1017/qua.2018.122
- Urrutia, B. M., Le Roux, V., Jagoutz, O., Müntener, O., Behn, M. D., and Chin, E. J. (2022). High water content of arc magmas recorded in cumulates from subduction zone lower crust. *Nat. Geosci.* 15 (6), 501–508. doi:10.1038/s41561-022-00947-w
- Urrutia, J., Herrera, C., Custodio, E., Jódar, J., and Medina, A. (2019). Groundwater recharge and hydrodynamics of complex volcanic aquifers with a shallow saline lake: Laguna Tuyajto, Andean Cordillera of northern Chile. *Sci. Total Environ.* 697, 134116. doi:10.1016/j.scitotenv.2019.134116
- Valdés-Pineda, R., Cañón, J., and Valdés, J. B. (2018). Multi-decadal 40-to 60-year cycles of precipitation variability in Chile (South America) and their relationship to the AMO and PDO signals. *J. Hydrology* 556, 1153–1170. doi:10.1016/j.jhydrol.2017.01.031
- Valdivielso, S., Hassanzadeh, A., Vázquez-Suñé, E., Custodio, E., and Criollo, R. (2022). Spatial distribution of meteorological factors controlling stable isotopes in precipitation in Northern Chile. *J. Hydrology* 605, 127380. doi:10.1016/j.jhydrol.2021.127380
- Valdivielso, S., Vázquez-Suñé, E., and Custodio, E. (2020). Origin and variability of oxygen and hydrogen isotopic composition of precipitation in the Central Andes: a review. *J. Hydrology* 587, 124899. doi:10.1016/j.jhydrol.2020.124899
- Vásquez, P., Sepúlveda, F. A., Quezada, A., Aguilera, S., Franco, C., and Blanco, N. (2018). “Cartas Guanillos del Norte y Salar de Llamara, Regiones de Tarapacá y Antofagasta,” in *Servicio Nacional de Geología y Minería, Carta Geológica de Chile, Serie Geología Básica* (Santiago, 195–196, 93 págs., 1 mapa escala 1: 100.000.
- Veloso, E. E., Tardani, D., Elizalde, D., Godoy, B. E., Sánchez-Alfaro, P. A., Aron, F., et al. (2020). A review of the geodynamic constraints on the development and evolution of geothermal systems in the Central Andean Volcanic Zone (18–28 Lat. S). *Int. Geol. Rev.* 62 (10), 1294–1318. doi:10.1080/00206814.2019.1644678
- Viguier, B., Daniele, L., Jourde, H., Leonardi, V., and Yáñez, G. (2019). Changes in the conceptual model of the Pampa del Tamarugal Aquifer: implications for Central Depression water resources. *J. S. Am. Earth Sci.* 94, 102217. doi:10.1016/j.jsames.2019.102217
- Villablanca, D. (2009). “Estudio de la relación isotópica δ18O/δ2H de los manantiales en el sector de las nacientes del Loa, Región de Antofagasta,” in *XII congreso geológico Chile*, 22–26.
- Villafañe, P. G., Frias-Saba, R. D. C., Della-Vedova, M., Citton, P., Díaz-Martínez, I., Valais, S. D., et al. (2023). Microbialite deposits of the Yacoraite Formation, NW Argentina: distribution, environments, paleoecology, and economic implications. *Braz. J. Geol.* 52. doi:10.1590/2317-488920220210088
- Villagrán, C., Armosto, J. J., and Kalin Arroyo, M. T. (1981). Vegetation in a high andean transect between Turi and Cerro Leon in northern Chile. *Vegetatio* 48, 3–16. doi:10.1007/BF00117356
- Voigt, C., Klipsch, S., Herwartz, D., Chong, G., and Staubwasser, M. (2020). The spatial distribution of soluble salts in the surface soil of the Atacama Desert and their relationship to hyperaridity. *Glob. Planet. Change* 184, 103077. doi:10.1016/j.gloplacha.2019.103077
- Vuille, M., and Ammann, C. (1997). Regional snowfall patterns in the high, arid Andes. *Clim. change* 36 (3–4), 181–191. doi:10.1007/978-94-015-8905-5_10
- Vuille, M., Bradley, R. S., and Keimig, F. (2000). Interannual climate variability in the Central Andes and its relation to tropical Pacific and Atlantic forcing. *J. Geophys. Res. Atmos.* 105 (D10), 12447–12460. doi:10.1029/2000JD900134
- Wang, F., Michalski, G., Seo, J. H., and Ge, W. (2014). Geochemical, isotopic, and mineralogical constraints on atmospheric deposition in the hyper-arid Atacama Desert, Chile. *Geochimica Cosmochimica Acta* 135, 29–48. doi:10.1016/j.gca.2014.03.017
- Wang, H., Huisman, R. S., and Rondenay, S. (2019). Water migration in the subduction mantle wedge: a two-phase flow approach. *J. Geophys. Res. Solid Earth* 124 (8), 9208–9225. doi:10.1029/2018JB017097
- Ward, K. M., Zandt, G., Beck, S. L., Christensen, D. H., and McFarlin, H. (2014). Seismic imaging of the magmatic underpinnings beneath the Altiplano-Puna volcanic complex from the joint inversion of surface wave dispersion and receiver functions. *Earth Planet. Sci. Lett.* 404, 43–53. doi:10.1016/j.epsl.2014.07.022
- Welch, C., Cook, P. G., Harrington, G. A., and Robinson, N. I. (2013). Propagation of solutes and pressure into aquifers following river stage rise. *Water Resour. Res.* 49 (9), 5246–5259. doi:10.1002/wrcr.20408
- Wittenberg, H. (1999). Baseflow recession and recharge as nonlinear storage processes. *Hydrol. Process.* 13 (5), 715–726. doi:10.1002/(sici)1099-1085(199904)13:5<715::aid-hyp775>3.0.co;2-n
- Yao, L., Sankarasubramanian, A., and Wang, D. (2021). Climatic and landscape controls on long-term baseflow. *Water Resour. Res.* 57 (6), e2020WR029284. doi:10.1029/2020WR029284
- Youngman, K. J. (1984). *Hydrothermal alteration and fluid-rock interaction in the El Tatio geothermal field, Antofagasta Province, Chile*. Master Thesis. The University of Auckland.
- Zandt, G., Leidig, M., Chmielowski, J., Baumont, D., and Yuan, X. (2003). Seismic detection and characterization of the Altiplano-Puna magma body, central Andes. *Pure Appl. Geophys.* 160, 789–807. doi:10.1007/978-3-0348-8010-7_14
- Zellmer, G. F., Edmonds, M., and Straub, S. M. (2015). Volatiles in subduction zone magmatism. *Geol. Soc. Lond. Spec. Publ.* 410 (1), 1–17. doi:10.1144/SP410.13